Spring 4-16-2019

Metabolon-Inspired Design of Multi-Modal Catalytic Cascade

Madelaine Seow Chavez
University of New Mexico - Main Campus

Madelaine S. Chavez

Candidate

Chemical and Biological Engineering

Department

This dissertation is approved, and it is acceptable in quality and form for publication:

Approved by the Dissertation Committee:

Prof. Plamen Atanassov ,Chairperson

Prof. Fernando Garzon

Prof. Ivana Matanović

Prof. Andrew Shreve

Prof. Mehran Tehrani

Metabolon-Inspired Design of Multi-Modal Catalytic Cascade

by

Madelaine S. Chavez

B.S., Chemical Engineering, University of New Mexico, 2016
M.S., Chemical Engineering, University of New Mexico, 2018

DISSERTATION

Submitted in Partial Fulfillment of the
Requirements for the Degree of

Doctor of Philosophy
Engineering

The University of New Mexico
Albuquerque, New Mexico

May, 2019

Dedication

To my dad and my best friend

Acknowledgements

The work presented in this dissertation was completed at the University of New Mexico. This study was supported by the Army Research Office Multidisciplinary University Research Initiative (#W911NF1410263) grant.

I would first like to thank my advisor, Dr. Plamen Atanassov, for the opportunity he has given me over the past 5 years not only as an undergraduate but as a graduate student as well for his guidance and mentorship. I would also like to thank Dr. Ivana Matanović, my graduate mentor, throughout my entire graduate career. She taught me many valuable skills I could not have learned anywhere else. Also, my secondary mentors, Dr. Nalin Anderson, Dr. Tristan Asset, and Dr. Stacy Copp for their guidance, knowledge, and collaboration.

I would also like to thank Dr. Shelley Minteer for her knowledge and collaboration throughout the whole of this project as well as Dr. Fernando Garzon, Dr. Mehran Tehrani, and Dr. Andrew Shreve for serving as members on my committee.

My experimental work would not have been possible without the use of catalysts, which were provided for me. Thank you to Dr. David Hickey, Dr. Sofiene Abdellaoui, and Vicotria Russel for synthesizing and sending me pyrene-TEMPO, OxDC, and $OxDC_{MUT}$ respectively, from the University of Utah.

I would like to thank the faculty and staff of the Chemical and Biological Engineering Department and the Center for Microengineered Materials.

I would like to acknowledge my friends and family who have continuously encouraged me. My father who has served as the ideal role model, taught me to never give up and do your best in every situation you are faced with. He was also a licensed professional engineer and chief engineer, which has served as a sign of hope that one day we all get to the place we want to be. My encouraging best friend, Jake. Even though he pursues different and challenging goals as a medical doctor, he has always given me encouragement to keep going.

I would also like to thank Dr. Frank Wyant at the Retinal Center and Dr. Donna Grace.

“You’re responsible for the effort not the result. Do your best in every situation and things will work out.”

Metabolon-Inspired Design of
Multi-Modal Catalytic Cascade

by

Madelaine S. Chavez

B.S., Chemical Engineering, University of New Mexico, 2016
M.S., Chemical Engineering, University of New Mexico, 2018

Ph.D., Engineering, University of New Mexico, 2019

Abstract

Developing hybrid catalytic systems has been researched for the past decade in an effort to efficiently incorporate catalysts of different modalities in catalytic cascades. It has become imperative to design a cascade system where the catalysts are spatially organized to control the delivery of precursors, intermediates, and products. In this work, we have shown that a molecular catalyst, biocatalyst, and metallic catalyst can be co-localized using a carbonaceous support to create a hybrid catalytic system and complete the oxidation of oxalic acid to create a microchemical reactor. The molecular, pyrene-TEMPO catalyst oxidizes glyoxalic acid to oxalic acid. The enzyme oxalate decarboxylase from *Bacillus Subtilis* is being used to convert oxalic acid

to formic acid followed by formic acid oxidation to CO_2 by the metallic catalyst, gold nanoparticles. This work continues to demonstrate incorporating these three catalysts of these three distinct modalities on the same support to catalyze a three-step catalytic reaction as a fundamentally new result. Finding the optimal ways to incorporate three catalysts with different modalities on the same support is expected to lead to the novel pathways in the design of synthetic multi-step cascade reactions towards the development of microchemical reactors.

This work is a contribution to the fundamental science behind developing hybrid catalysts of distinctly different modalities and their use in multi-step catalytic reactions. One of the main technical contributions of this work in creating a synthetic catalytic cascade was by immobilizing metallic nanoparticles, molecular redox catalysts, and an enzyme in the same carbonaceous support and demonstrating the synergistic effect of their co-presence in an overall catalytic reaction enhancement. This research opens paths to develop and engineer more complex synthetic hybrid catalysts for larger multi-step cascade reactions as well as the development of more sophisticated microchemical reactors, which include using different catalysts and different alternative fuels.

Table of Contents

List of Figures

List of Tables

Abbreviations

AuNP	Gold Nanoparticles
3D-GNS	3-Dimensional graphene nanosheets
CPB	Citric phosphate buffer
CV	Cyclic Voltammogram
FA	Formic acid
FDH	Formate dehydrogenase
GA	Glyoxalic Acid
GOx	Graphene Oxide
MWNT	Multi-walled carbon nanotube
OA	Oxalic Acid
OxDC	Oxalate Decarboxylase
$OxDC_{WT}$	Oxalate Decarboxylase Wild Type
SERS	Surface Enhanced Raman Spectroscopy
PBSE	1-pyrenebutyric acid N-hydroxysuccinimide ester
PdNP	Palladium Nanoparticle
TBAB	tetrabutylammonium bromide Nafion
TEMPO	2,2,6,6-(tetramethylpiperidin-1-yl)oxyl

Chapter 1

Introduction

The use of fossil fuels, such as oil, coal, and natural gas, for current energy conservation and chemical processes relies primarily on their combustion in air or with oxygen derived from air, at power plants, to provide heat. Fossil hydrocarbon sources employed as a feedstock in chemical industry are being thermally activated, thus requiring more fossil fuels for its conversion, thus placing yet another branch of technology in its dependence.

These fossil fuels and hydrocarbon sources used in both power and heat generation, transportation and as a source of chemical in synthesis are non-renewable, limited resources. Their use is predominantly, in gas phase, elevated temperature, and as it is being conducted on a large scale they preset the largest component of current man-made heat and CO_2 production. Technology is moving towards developing multi-step reactions on a condensed size. As a part of overcoming total reliance on fossil fuels, a new technology is emerging dependent on the development of multi-step reactions, carried out with catalytic processes in condensed/ liquid phase and allow (or lower) temperatures. These new generation of chemical reactions tend to rely on development of the process based on light or electrochemical opposed to thermally or under high pressure. Such technology is aiming to replace large scale reactor units, with desirably more flexible, smaller scale distributed chemical technology, relying on heterogeneous liquid phase reactors operating at room temperature. Ultimately, such processes should not require fossil fuels or a fossil feedstock but O_2 capture on energy from renewable sources. This vision integrates hydrogen

economy with carbon-neutral technology and fuel electrosynthesis with electrolysis and hydrogen fuel cells [1].

One of the complex alternative fuels is biodiesel, produced from algae or plant-generated fatty acids. One of the main byproducts during production of biodiesel is glycerol obtained in the process of hydrolysis of triglycerides, from which fatty acids are being derived. For every 100 kilograms of biodiesel produced, it yields 10 kilograms of crude glycerol (also known as glycerin).

In nature multi-step catalytic reactions are carried out on assemblies of enzymatic catalyst, quaternary protein structures, in which the constituent enzymes are assembled in physical proximity and in exact, specific special orientation to each other to catalyze the consecutive processes. Such dynamic structures, that specifically exist in organelles responsible for complex metabolic processes (like the mitochondria or thylakoids), are called *metabolons*. This dissertation central synthetic idea rests on the notion of "artificial metabolon." This is a biomimetic/bioinspired concept, which postulates that ensuring spatial proximity and cooperation of catalysts with distinctly different modality (type, nature structure) is a critical step towards building multi-stage catalytic chemistries for liquid-phase chemical processes. Constructing cascade heterogenous reaction with different modalities, "artificial metabolons", is one pathway that leads to low temperature cascade reaction that ultimately could impact the entire field of chemical engineering. The focus of this dissertation will be primarily on biological catalysts (enzymes), molecular catalysts

(organocatalysts), and metallic (nanoparticle) catalysts to develop a synthetic multi-step catalyst cascade system inspired by metabolons as a concept.

Importance of Catalytic Systems for Multi-Step Cascades

Metabolons were observed in nature and the system of these enzymes convert precursors to desires products. Researchers suggest the existence of preferential intermolecular interactions between sequential enzymes of metabolic pathways often termed a metabolon; a multienzyme complex. There is a specific type of conversions in these systems, called substrate channeling, where the binding sites of the enzymes are in close proximity and the precursors can be shuttled from one enzyme to the next without diffusing into the bulk solution [2,3].

Glycerol was chosen as the fuel for the cascade because it is abundant, an alternative fuel, readily available, has a high energy density, and is inexpensive [4,5]. It is a byproduct from the Biodiesel production; an alternative fuel. The oxidation of glycerol will serve as the model cascade that will be used towards this research (Figure 1-1). This cascade reaction has been used studied by other groups with the use of enzymatic, molecular, and hybrid enzymatic-molecular catalysts. Enzyme cascades were recently been studied towards the use of biofuel cells where compartmentalization and a multienzyme complexes were used to complete the oxidation of glycerol. However, there are challenges with the stability and the specificity of enzymes utilized [6,7,8].

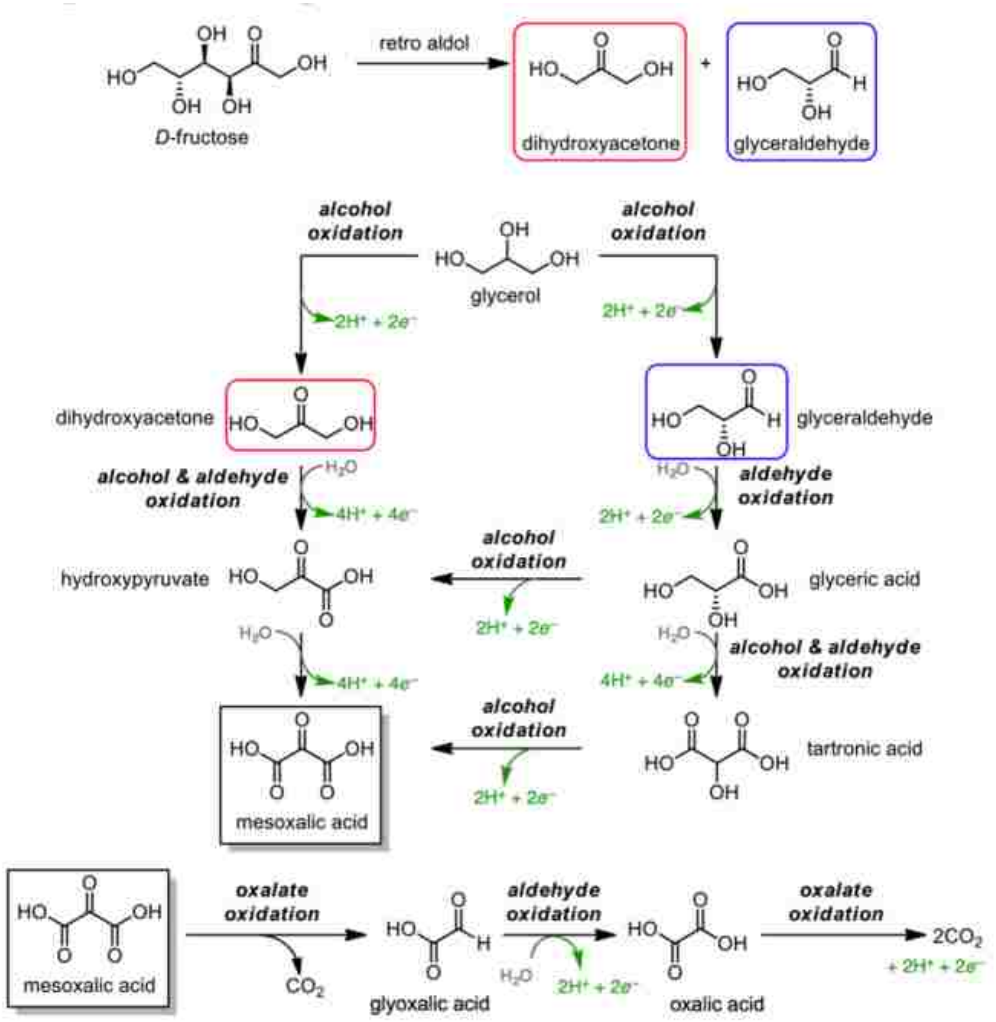

Figure 1- 1: Multi-step fructose oxidation cascade

In the glycerol oxidation cascade, there is a problematic step which involves breaking the C-C bonds in oxygenated molecules, which only enzymes and inorganic catalysts can perform. A combination of the three types of catalysts promises to create a complex system that can mimic natures solution of creating metabolons [9,10,11]. This complex system of catalysts promises to produce multi-step chemical cascade reactions that effectively control the flux of precursors, intermediates, and products.

The catalyst works by reducing the activation energy necessary to form reaction intermediates. In doing so, they increase the rate at which the thermodynamically favored products are formed (Figure 1-2).

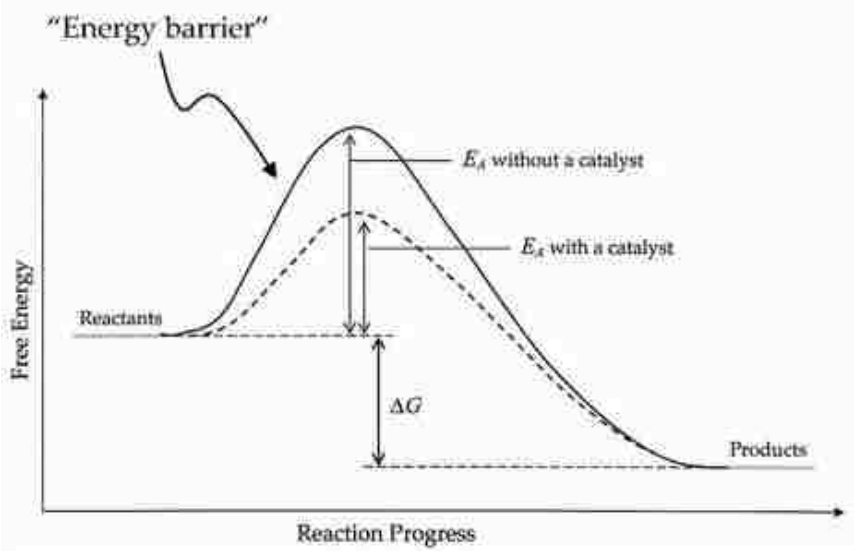

Figure 1- 2: Example of Free energy vs Reaction coordinate diagram showing the difference using a catalyst vs no catalyst in activation energy.

Enzymatic Catalyst

Enzymatic catalysts increase the rate of a chemical reaction in the active site of a protein. They lower the activation energy of a reaction by providing the reaction with an alternative route to form reaction intermediates and in doing so, increase the rate at which the thermodynamically favored products are formed (Figure 1-2). They can be part of a multi-subunit complex or associated with a co-factor reaction. These catalysts, unlike others, are not consumed in the reaction and therefore can perform multiple catalysis. Enzymatic catalysts are very fragile, but they are able to catalyze the breaking of C-C bonds in cascade systems. Enzymes are powerful catalysts for use in electrochemical systems for a number

of reasons. They have high selectivity for reactants (substrates); they are active only towards specific substrates. Their activity remains high in dilute acidic or neutral solutions as well as at temperatures close to room or slightly above. They also have a very high specific activity per active site (high turn-over).

Enzymatic catalysts are known to follow the Michaelis-Menten model which describe the enzyme kinetics This is the rate of enzymatic catalytic reactions (U) can be described in terms of the substrate concentration [S] as follows:

$$U = \frac{V_{max} * [S]}{k_M + [S]} \quad (1)$$

V_{max} represents the maximum rate achieved by the system, at saturating substrate concentration [S]. The Michaelis constant, k_M, is the substrate concentration at which the reaction rate is half of V_{max} (Figure 1-3).

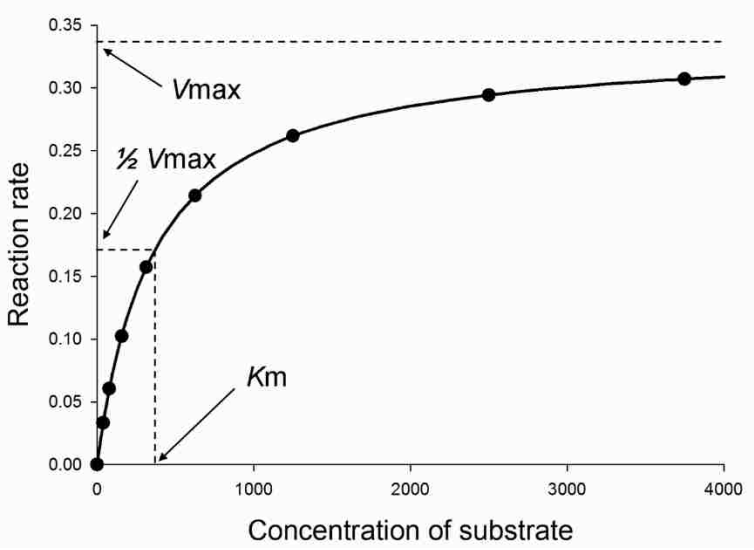

Figure 1- 3: Example of a Michaelis-Menten plot

Molecular/ Organic Catalyst

The term organo-catalysis (molecular catalysis) refers to a form of catalysis, where the rate of a chemical reaction is increased by an organic catalyst. This catalyst consists of carbon, hydrogen, sulfur and other nonmetal elements found in organic compounds. They are oxidation catalysts that are capable of catalyzing the oxidation of multiple oxygen-containing functional groups. There are also advantages to using an organic catalyst. There is no need for the use of metal-based catalysis thus making a contribution to green chemistry.

Metallic/ Inorganic Catalyst

An inorganic catalyst is a substance with catalyzing properties that lacks carbon-carbon and carbon-hydrogen bonds, such as the elements platinum and rhodium. Commonly used catalysts for the oxidation of intermediates in the glycerol cascade are based on platinum and Pt-based alloys [12]. However, platinum can become deactivated due to the formation of an oxide layer, and/or poisoned in the presence of organic molecules and intermediates that are generated in the oxidation process [13]. It has been shown that when oxalic acid is reduced on the surface of Pt (110), it leads to the formation of irreversibly bonded CO, which poisons the catalyst. Other studies have shown that on Pt electrodes, mesoxalic acid is being oxidized through an irreversible four electron reaction. These limitations can be overcome by several alternatives, which include Pd and Pd-based alloys. These catalysts are characterized with superior performance for the selective oxidation of alcohols, such

as ethanol, lower costs and reduced CO_{ads} poisoning effect [14,15,16]. The metallic catalyst that will be used and incorporated into this system is gold and gold nanoparticles and have shown to be active towards the oxidation of glycerol [17]. More specifically it has been shown to be active towards the ending intermediates of the glycerol cascade.

Hybrid Enzymatic-Molecular Catalyst Systems

There has been previous work done towards the combination of a hybrid enzymatic-molecular catalyst system [18,19,20]. It has been demonstrated that the enzyme oxalate oxidase (OxOx) and the molecular catalyst amino-TEMPO (TEMPO-NH_2) are able to catalyze the oxidation of the glycerol. In this cascade reaction, TEMPO-NH_2 oxidized glycerol to mesoxalic acid and OxOx in the combination with TEMPO-NH_2 was used to oxidize mesoxalic acid all the way to CO_2. However, this system had limitations which included low enzyme specific activity, low substrate range of the enzyme and incompatibility pH range between the two catalysts. OxOx and its cupin superfamily enzymes are optimized to function in pH 4 and TEMPO functions in pHs higher the 4. The overlapping pH range was studied for these two catalysts and the pH was determined to be pH 5.2 (Figure 1-4).

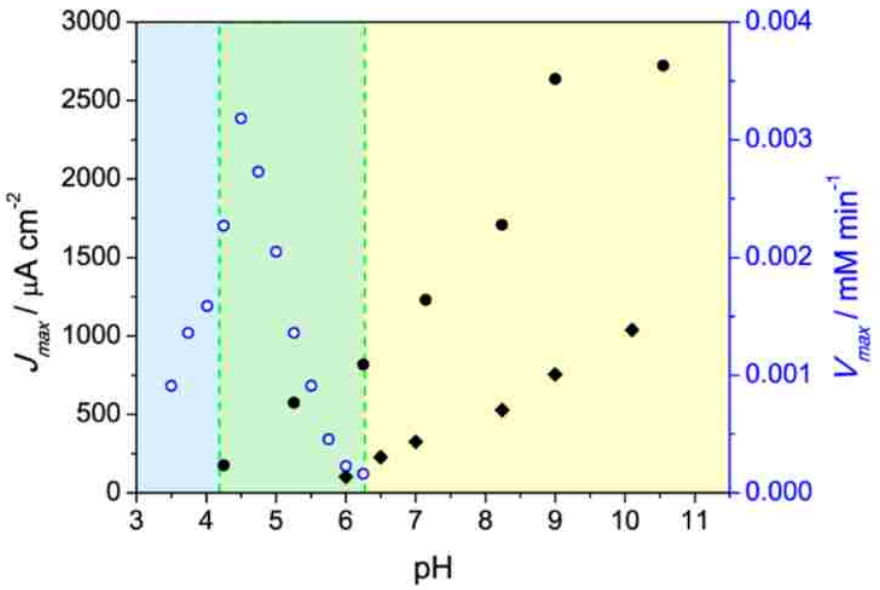

Figure 1- 4: Overlapping pH profile range for oxalate oxidase (open circle), TEMPO (diamond), TEMPO-NH_2 (solid circle). Dotted lines indicate overlapping pH range [19].

These two catalysts were not co-localized on a support to carry out a multi-step reaction but instead was carried out by bulk electrolysis of a solution containing both the enzymatic and organic catalysts [19].

It was found that there is low compatibility of the pH range between the TEMPO-NH_2 and OxOx so further research was made to oxidize glycerol. OxOx was replaced with oxalate decarboxylase (OxDC). In this reaction scheme, TEMPO-NH_2 oxidized glycerol to mesoxalic acid, and a combination of TEMPO-NH_2 and OxDC transformed mesoxalic acid to glyoxylic acid, oxalic acid, formic acid, and then to CO_2. It was found that the current density of the OxDC increased 8 times and is compatible with TEMPO-NH_2 at a larger pH range when compared to OxOx. The products were measured with HPLC and ^{13}C-NMR[20]. This information helped guide the direction of this proposal namely that the same two catalyst were used to develop a hybrid catalyst.

Hybrid enzymatic-metallic catalytic system

Similar to the enzymatic-molecular catalyst, a hybrid enzymatic-metallic catalyst was also explored previously. OxDC was used as the enzymatic catalyst and PdNP was used for the metallic catalyst co-localized on 3D-GNS. OxDC natural substrate is oxalic acid and Pd is a less selective catalyst. It is able to oxidize a range of the substrates in the glycerol cascade. OxDC converts oxalic acid to formic acid and PdNPs oxidize formic acid to CO_2 in pH 5.2 as well. The combination of the two catalysts were able to carry out a two-step subsequent reaction.

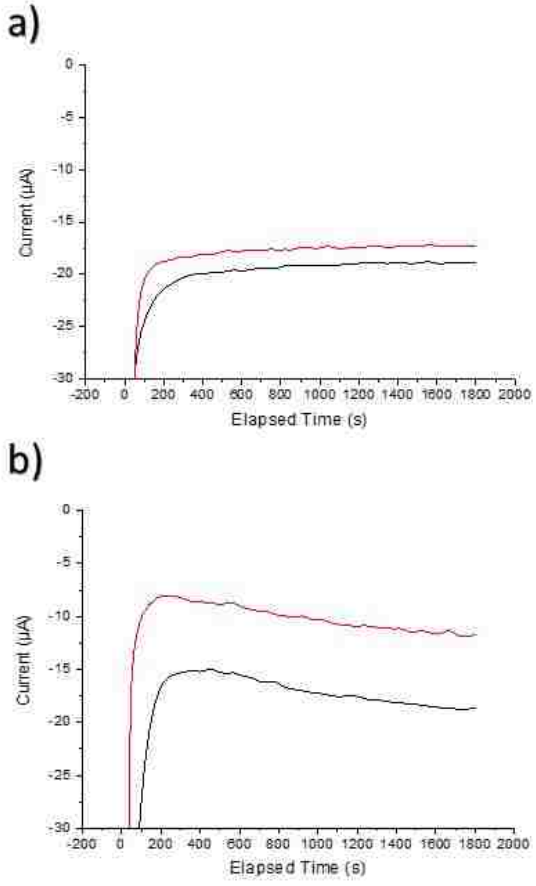

Figure 1- 5: Chronoamperogram Activity for a) Pd/3D-GNS in the presence of oxalic acid (red) and b) OxDC/Pd/3D-GNS in the presence of oxalic acid (red) at pH 5.2 in 0.1 M citric phosphate buffer at 25°C

The two catalysts were both spatially organized on the same support instead of in bulk electrolysis, however, the system was not optimized which resulted in slightly higher activity of the hybrid catalyst when compared to the single catalyst. Furthermore, it was not shown how effectively the enzyme was immobilized to the carbon support.

This has also been demonstrated by Engstrom, et al. where they immobilized an enzyme and a nanometal species into the cavity of a mesoporous heterogeneous support. This co-immobilization method was demonstrated by the dynamic kinetic resolution (DKR) of a primary amine, which was used as a model reaction. The reactant 1-phenylethylamine, racemic amine, entered the cavity support and was exposed to the enzyme *Candida antarctica* lipase B. This led to the selective acylation of the (R)-enantiomer of the amine. The (*R*)-amide exited the cavity and the (*S*)-enantiomer of the amine was racemized by nanopalladium inside the cavity. The racemic amine formed again, and the reaction was repeated.

Chapter 2

Problem Statement and Objectives

The production of fossil fuels and renewable fuels have their own advantages and disadvantages. Some of the disadvantages in a developing work of technologies are that the use of these fuels is most of the time thermodynamic, which means takes place at a high temperature. They are also conducted on a macro scale, in gas phase, and are sometimes fossil fuels/non-renewable fuel sources. The primary objective of the work described in this proposal is to explore the fundamental research to develop a hybrid catalyst that can catalyze a multi-step cascade reaction but on a micro scale to develop the beginnings of a microchemical reactor. This idea is inspired by a phenomenon in nature observed as metabolons.

The incorporation of catalysts of different modalities on the same support presents several challenges from several perspectives. These involve the engineering of a system to spatially organizing these catalysts on the same support in which they cooperate to provide one product to the next catalyst. Each catalyst can function on its own, however when incorporating more than one catalyst of different modalities, each catalyst functions in a set of parameters or optimal environmental settings. The challenge will be in finding one environment in which all the catalysts can co-exist and can function efficiently while being immobilized on the same support.

The model cascade that will be used was mentioned before, oxidation of glycerol however, this research will focus on the last three steps of the glycerol cascade. The goal is to design chemical processes to co-localize three catalysts of three different modalities on the same support while maintaining their activity. This also needs to be achieved at room temperature, on a small scale, and in liquid phase. The first reaction will be the oxidation of glyoxalic acid to oxalic acid by TEMPO. The second reaction will be catalyzed by OxDC, which converts oxalic acid to formic acid. The last reaction will be catalyzed by the AuNP, which will oxidize formic acid to CO_2. The reaction scheme is shown in Scheme 1. The primary objective of the work described in this proposal is to design and engineer a synthetic multi-step cascade reaction system. The completion of this fundamental research will demonstrate a small-scale reaction at room temperature in liquid phase by using electrochemical methods.

Engineering Objectives

Developing techniques towards designing a synthetic multi-step cascade reaction to mimic natures strategy of developing metabolons, which will lead to a cascade reaction undertaken on a small scale and in liquid phase at room temperature. The limitations and strengths of each catalyst will be studied, which will enable their successful incorporation in one hybrid catalyst.

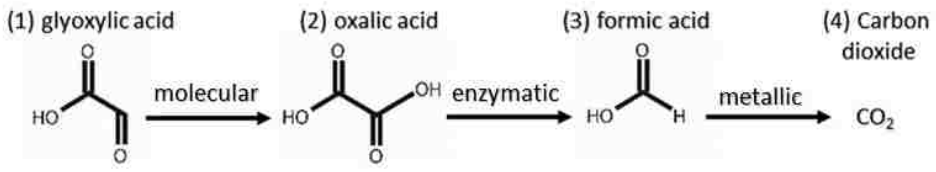

Scheme 1: The proposed multi-step cascade reaction of oxidation of glycerol. (1) glyoxylic acid, (2) oxalic acid, (3) formic acid, and (4) carbon dioxide.

- **Task 1: Immobilization of Oxalate Decarboxylase on 3D-GNS.**

A UV-Vis formic acid dehydrogenase-based assay will be used to determine if oxalate decarboxylase is immobilized to the carbonaceous support. The immobilization of oxalate decarboxylase will be designed and optimized using a tether, 1-pyrenebutyric acid n-hydroxysuccinimide ester (PBSE). The immobilization of OxDC will first be demonstrated on a simple support and the technique will then be translated to a complex support; 3D-GNS and tested using the same UV-Vis FDH based assay. This assay will yield information on the kinetics of the enzyme to determine which loading of PBSE is optimal for immobilization.

- **Task 2: Design of Hybrid Enzymatic-Molecular Catalyst on 3D-GNS**

As a result, from Task 1, OxDC will be immobilized to a complex support such as 3D-GNS and can successfully convert oxalic acid to formic acid. As a part of Task 2, pyrene-TEMPO, an organocatalyst, will be immobilized onto 3D-GN. As a next stage, both OxDC and pyrene-TEMPO will be immobilized to 3D-GNS so that they can perform a two-step hybrid cascade reaction of oxalic acid to formic acid to CO_2. A simple electrochemical

technique will be employed to determine the current densities of the hybrid system to determine the completion of the two-step cascade reaction.

- **Task 3: Hybrid Enzymatic-Molecular-Metallic Catalyst on 3D-GNS**

The objective is to successfully incorporate three catalysts, pyrene-TEMPO, OxDC, and AuNPs onto 3D-GNS in order to catalyze the three-step reaction of glyoxalic acid oxidation. Three catalysts of three different modalities supported on the same platform have never been incorporated in such a way to complete a catalytic cascade. Each catalyst thrives in different conditions such as pH and temperature or is active at different potentials. The goal is to discover one environment in which these catalysts are still active and can oxidize glyoxalic acid to CO_2 while being supported on the scaffold.

- **Task 4: Incorporation of Microchemical Reactor**

The objective for this last objective is to further actualize reactions on a smaller scale by incorporating the use of a microchemical reactor. The hybrid catalysts will function as the working electrode on the reactor that will have windows for SERS detection zones. This technique will allow for the determination of the analytes before and after the reaction has proceeded to analyze the products formed in the effluent. This SERS detection zones will be analyzed by using a Raman microscope.

Chapter 3

Experimental Methods

UV-Visible Spectroscopy

Ultraviolet-visible spectroscopy is a spectroscopy technique that refers to the absorption or reflectance spectroscopy in the ultraviolet-visible light spectral region. Molecules that contain electrons (non-binding electrons) can absorb energy in the form of ultraviolet or visible light. The electrons are excited to a higher anti-bonding molecular orbital. If the electrons are easily excitable, the longer the wavelength of light it can absorb. The intensity of light passing through a sample can be measured by a UV-Vis spectrophotometer. To determine the absorbance of a sample, the Beer-Lambert law can be used, which states that the absorbance of a solution is directly proportional to the concentration of the absorbing species in the solution and the path length. For a given path length, UV/Vis spectroscopy can be used to determine the concentration of the absorber in a solution.

Cyclic Voltammetry

The system is characterized by varying the current and measuring the resulting change in potential. This is operating as a galvanostatic cell or galvanodynamic regime. A single electrode (anode or cathode) is operated in half cell in what is known as a three-electrode mode. In this cell set up, the electrode being characterized is the working electrode, and operating opposite to it is a counter electrode composed of a high activity material like Pt

that can complete the circuit, by catalyzing the conversion of H^+ and e^- to H_2. Between the working and counter electrodes is a reference electrode with a known potential. This allows for the relative potential of the working electrode to be determined and controlled.

All electrochemical experiments were performed with a three-electrode half-cell consisting of a glassy carbon working electrode, a platinum counter electrode and a Ag/AgCl reference electrode. Cyclic voltammetry (CV) is used to determine the oxidation-reduction reactions that occur on an electrocatalyst. Cyclic voltammetry is a very useful electrochemical characterization technique that determines the behavior of oxidation-reduction reactions that occur on an electrocatalyst. A potentiostat applies a potential that varies with time. The potential follows a triangular waveform that varies as a function of the potential range as well as the rate of change in potential.

Synthesis of Modified Graphene Nanosheet Supports

The Graphene nanosheets were synthesized by adopting the modified Hummer Method [21]. Graphite flakes were intercalated and oxidized to yield Graphene Oxide (GOx). The GOx was then washed with DI water and centrifuged at 3500 rpm twice followed by exfoliation in a water solution using a high-power ultrasonic probe.

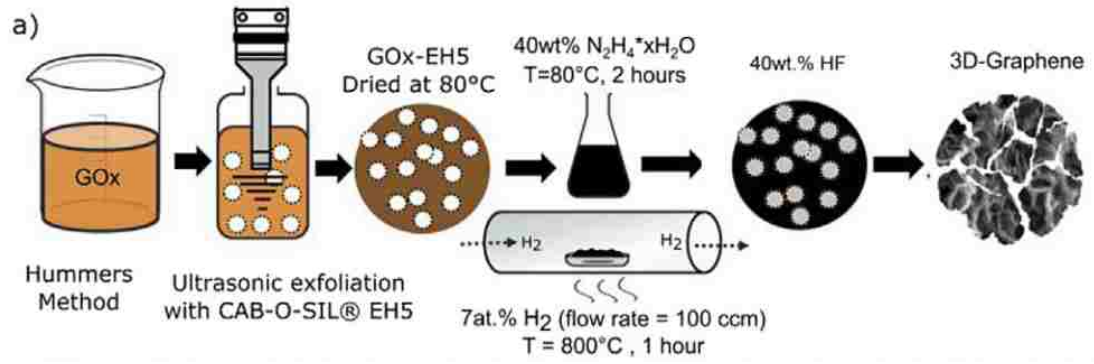

Figure 3- 1: Illustration of chemically and thermally reduced 3D graphene nanosheet supports synthesized using the sacrificial support method.

Sacrificial Support Method (Templating)

20 g of fumed silica sacrificial template EH5 (Cab-O-Sil® EH5, surface area ~ 400 m^2 g^{-1}, 0.14 mm size of agglomerates) was infused with 10 g of GOx exfoliated mixture (2:1 weight ratio). The infused GOx-EH5 exfoliated mixture can then be divided into two batches and reduced further to GNS using thermal or chemical reduction methods.

Thermal Reduction

The GOx-EH5 exfoliated mixture was dried in an oven operating at T = 85°C overnight. It was then ball-milled at 400 RPM for 15 min and subjected to thermal reduction in 7 at % H_2 (flow rate = 100 ccm) at T = 800°C for 1 h).

Acid Etching of the Sacrificial Template

The resulting batches of dried powder obtained from a thermally reduced sample were then leached with 25 wt.% HF overnight [22]. This is done to remove the sacrificial (EH5) template [21,22]. The black suspension was then washed by centrifugation until it reached a neutral pH, followed by overnight drying at T = 85°C. This resulted in the final material used as the support in which the catalysts were immobilized.

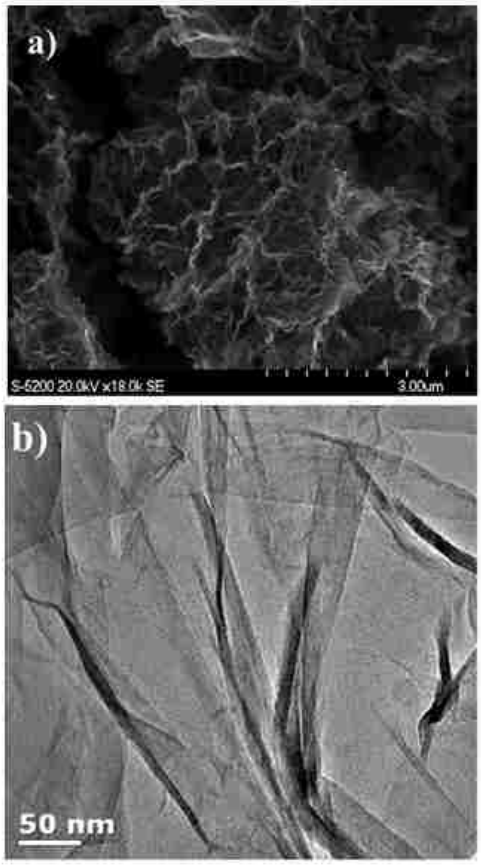

Figure 3- 2: Illustration of thermally reduced 3D graphene nanosheet supports synthesized using the sacrificial support method.

Chapter 4

Immobilization of Oxalate Decarboxylase on Carbonaceous Supports

The first objective of this project was to immobilize an enzyme to a carbonaceous support. The enzyme chosen is a large hexameric enzyme, Oxalate decarboxylase (OxDC) from *Bacillus subtilus*. OxDC belongs to cupin superfamily. It catalyzes the cleaving of the C-C bond in oxalic acid to form formic acid and CO_2 and requires molecular oxygen for a catalytic turnover. It is a large hexameric, approximately 12-13 nm across in diameter, enzyme with a quaternary structure of two homotrimers (Figure 4-1). As each monomer contains two Mn-binding sites (orange spheres); the entire enzyme contains twelve Mn-binding sites. It functions under oxygenated conditions. It is easily expressed through E. coli, has high specific activity, and offers advantages in terms of cost and possibility of enzymatic engineering. [23,24].

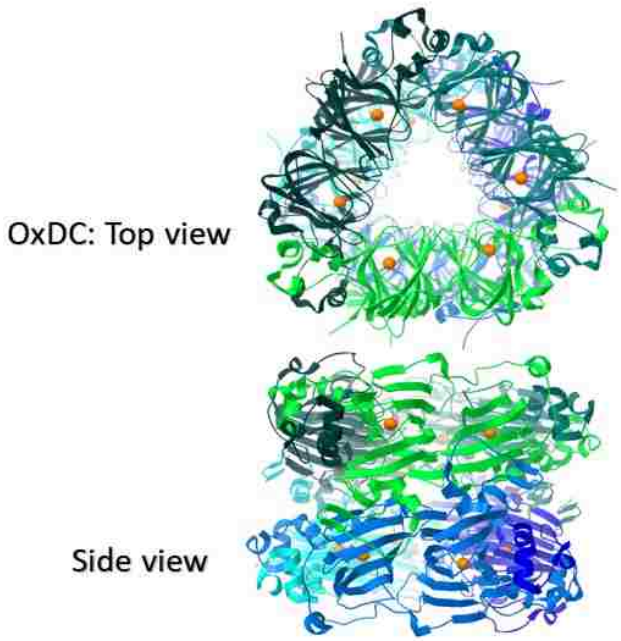

Figure 4- 1: Ribbon representation of the oxalate decarboxylase trimer in which the enzyme monomers are shown in different hues of green and blue (top view) from the high-resolution crystal structure of *B. subtilis*. Bound Mn(II) ions are shown as orange spheres. In the biologically active form of the enzyme, two trimers are packed together to give a hexamer quaternary structure (side view).

OxDC has been immobilized before to the membrane of the CO_2 sensor, Eupergit, and Zn-IMAC resin either by entrapment or by covalent attachment [25,26,27]. Our group has immobilized enzymes before using a tethering technique with 1-pyrenebutyric acid *N*-hydroxysuccinimide ester (PBSE). PBSE has been used by the Atanassov group to immobilize other enzymes such as bilirubin oxidase to multiwalled carbon nanotube bucky paper and horseradish peroxidase to carbonaceous platforms [28,29,30]. The pyrene moiety of PBSE π-π stacks with the carbon nanotubes and the head group makes amide bonds with the NH_2 groups on the enzyme. By tethering enzymes there is a low immobilization rate as well as decreased efficiency. OxDC is a large hexameric enzyme that requires complex immobilization techniques. OxDC has six subunits in its structure and subunit-subunit

interactions may be weakened by immobilization, which may cause the multimeric enzyme to dissociate resulting in rapid inactivation [31]. The kinetics of immobilized OxDC, using various concentrations of the tether, was studied in this first part of the project to determine how much tether would cause inactivation and how much tether was optimal for maximum activity. Scheme 4-1 depicts the reaction scheme that was used to determine the kinetics of OxDC. Oxalic acid is converted to formic acid by OxDC and formic acid is oxidized to CO_2 by FDH. The co-factor reaction that occurs when formic acid is oxidized to CO_2, in which NAD^+ oxidized to NADH is monitored using UV-Visible spectroscopy at 340 nm.

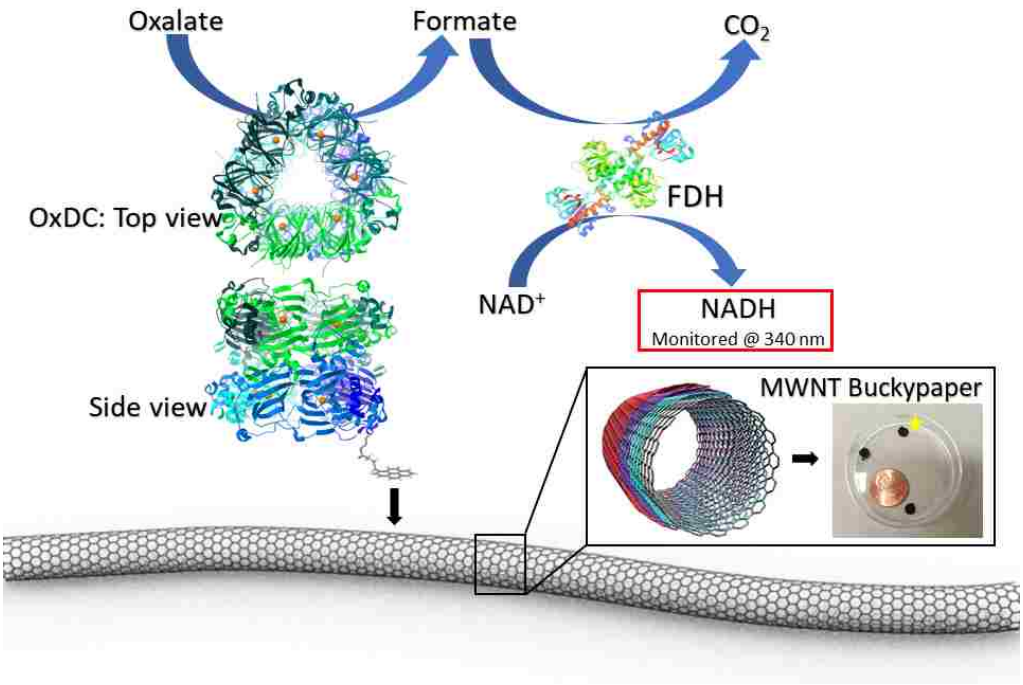

Scheme 4- 1: Schematic view of the FDH assay used to study the enzymatic properties of OxDC in solution and OxDC immobilized on multi-wall bucky paper. OxDC converts oxalic acid to formic acid. FDH converts formic acid to CO_2 while the co-factor reaction of NAD^+ oxidizes to NADH and is visible at 340 nm.

Expression/Purification of Oxalate Decarboxylase from *Bacillus Subtilis*

The oxalate decarboxylase (OxDC) gene from *Bacillus subtilis* was amplified using the high-fidelity AccuPrime™ Pfx DNA Polymerase using the plasmid pET-16b-OxDC. The template was supplied generously by Professor Steven Ealick from Cornell University (Ithaca, NY). The PCR was performed with T7 promoter primer (5'-TAATACGACTCACTATAGG-3') and T7 terminator primer (5'-GCTAGTTATTGCTCAGCGG-3'). The PCR product was digested by restriction enzymes, BamH1 and Nde1, and cloned into pET-9a expression vector (Novagen®, San Diego, CA), which was previously digested with the same restriction enzymes. The resulting plasmid (pET-9a-oxdc) was sequenced by the Health Science Core facility at the University of Utah which was used to transform E. coli BL-21(DE3). After selection onto Luria-Bertani (LB)-Agar in presence of 100 μg ml^{-1} kanamycin and chloramphenicol, one positive colony was inoculated into LB broth containing the same quantity of antibiotics and incubated at 37° C overnight. 20 ml was used to inoculate 2 L of LB broth and the resulting cultures were incubated at 37° C until an OD600nm of 0.5 was reached. To this, a heat shock of 42° C for 15 minutes was applied to the induction of the expression followed by the addition of 1 mM IPTG and 5 mM MnCl2. The induced cells were then incubated at 30° C for 4 h, while shaking. Cells were then harvested by centrifugation at 5000 g, during 15 min at 4° C, and re-suspended in 50 mM Tris-HCl (pH 7.0) followed by a mechanic disruption through two passages into microfluidizer (18,000 psi, at 4°C). After centrifugation at 10000 g for 15 min at 4° C, the soluble fraction of the cell lysate was applied to a Q-Sepharose Fast Flow column (2.5 cm x 25 cm) equilibrated with 50 mM

Tris-HCl (pH 7.0). Elution was performed using a 500 ml linear gradient from 0 to 1 M NaCl. The fractions contained purified OxDC was pooled and concentrated by ultracentrifugation in Amicon centrifugal filter (30 kDa, Millipore, Billerica, MA) to a final volume of 5 ml. The protein was then desalted using a Hitrap desalting column (5 ml, GE Healthcare) equilibrated with 50 mM phosphate buffer (pH 7) containing 100 mM NaCl. The resulting protein was flash frozen in liquid N^2 and stored at -80°C.

Multiwalled Carbon Nanotube Buckypaper

Circular disks (d = 2 mm) of multiwalled carbon nanotube (MWNT) buckypaper were cut and conditioned in 50, 100, 150, 200 mM PBSE for 1 hour, which was dissolved in ethanol and sonicated for 30 minutes prior. The MWNT buckypaper was rinsed in citric phosphate buffer (CPB) pH = 4 to remove any PBSE that was not attached. This also prepared the buckypaper for the enzyme instead of being washed in water. 10 µL of OxDC, from *Bacillus subtilis*, was dropped onto the MWNT buckypaper disk and is stored at 4°C for 16-18 hours covered to cure. Before experiments, the MWNT buckypapers were rinsed in CPB to eliminate enzyme that was not immobilized.

3-Dimensional Graphene Nanosheets Electrodes

The base ink consists of 5 mg of 3D-GNS were mixed into 925 µL of H_2O and 75 µL of TBAB Nafion (5 mg of TBAB Nafion in 63 µL of ethanol sonicated for 30 minutes) and was ultra-sonicated for 10 seconds to allow for dispersion. 40 µL of base ink was combined

with 10 μL of PBSE (150, 200 and 300 mM PBSE sonicated in ethanol for 30 minutes) and 2 μL of 2.3 mg/ml OxDC making the total volume 50 μL. 3uL of the combined ink was drop-casted onto a glassy carbon electrode and stored at 4°C for 16-18 hours to cure. The electrodes were rinsed with CPB to remove enzyme that was not immobilized before experiments.

Formic Acid Dehydrogenase Assay

Dilutions from 5 to 250 mM of formic acid in citric phosphate buffer (pH = 4) were placed in wells of a 96-well plate. 200 mM dipotassium phosphate was added followed by the addition of 100 mM NAD^+ and 2.5 U of FDH from *Candida boidinii*. UV-visible measurements were then taken using a Spectra Max $M2^e$ equipped with a plate reader at 340 nm.

Oxalate Decarboxylase Assay

Dilutions from 5 to 50 mM of oxalic acid in citric phosphate buffer (pH = 4) were placed in wells of a 96-well plate. The electrodes with immobilized enzymes were placed into each well of the different concentrations and incubated for 2 minutes. 200 mM dipotassium phosphate was added to quench the reaction followed by the addition of 100 mM NAD^+ and 2.5 U of FDH. UV-visible measurements were then taken using a Spectra Max $M2^e$ equipped with a plate reader at 340 nm.

Kinetics of Oxalate Decarboxylase in Solution

The FDH assay was used to determine and study the kinetics of OxDC in solution in which the Michaelis-Menten plot was obtained. The FDH assay was used to indirectly monitor the production of formic acid by OxDC. For formic acid to be consumed by FDH, a co-factor reaction takes place simultaneously where NAD^+ was consumed and converted to NADH. The assay quantitatively tracks the formation of NAD^+ to NADH in which formic acid was being oxidized to CO_2 by formic acid dehydrogenase using UV-Visible at 340 nm. The standard FDH assay curve was obtained from formic acid concentrations quantified using the slopes from the increase of absorbance using Beer's law:

$$A = \mathcal{E}LC \tag{2}$$

Knowing $\left(\frac{dA}{dt}\right)$, the slope that was observed during UV-Visible measurements and the extinction coefficient of NADH (6220 cm^{-1}) the concentration per time $\left(\frac{dC}{dt}\right)$ could then be calculated for each desired concentration using the differentiated Beer's law equation:

$$\frac{dA}{dt} = \mathcal{E}L\frac{dC}{dt} \tag{3}$$

This equation yields, $\left(\frac{dC}{dt}\right)$, which is also known as U or V in μmol min^{-1} after unit manipulation. This plotted against formic acid concentration yield a calibration curve. The calibration curve was fitted in Origin Pro to a Michaelis-Menten equation (Eq. 3) and yields the Michaelis-Menten constant, K_M, and maximum velocity, V_{max}, for each assay:

$$U = \frac{V_{max} * [formate]}{k_M + [formate]} \tag{4}$$

The values were then used to calculate the rate of OxDC in each assay. This was done by first calculating formic acid concentration using Eq. 4:

$$[S] = \frac{k_M * U}{V_{max} - U} \quad (5)$$

This was used to calculate formic acid quantity in μmol using Eq. 5 by dividing by the volume used in the 96-well:

$$Formate\ quantity = [S] * volume * 1000 \quad (6)$$

To obtain the rate of OxDC (μmol min^{-1}), this value was divided by the incubation time, in minutes, your rate of reaction:

$$Rate\ of\ OxDC = \frac{formate\ quantity}{incbation\ time} \quad (7)$$

The obtained values along with the concentration of oxalic acid were used to create a Michaelis-Menten plot. From the Michaelis-Menten plots, the Hanes-Woolf plots were derived to determine K_M and V_{max} of OxDC for each concentration of PBSE that was used to tether the enzyme. This was done using the same program Origin pro, fitted using its linear regression parameters. The V_{max} value obtained from the inverse of the slope and K_M was obtained from V_{max} multiplied by the y-intercept and then used to fit a Michaelis-Menten curve to the experimental data. These plots were determined for two different platforms; multiwalled carbon nanotube (MWNT) buckypaper and 3-dimensional graphene nanosheets (3D-GNS).

The kinetics of OxDC was first determined in solution (Figure 4-2) to compare with immobilized OxDC. Free enzyme was expected to have a higher activity than when it is immobilized and was more efficient at converting its substrates. The oxalate decarboxylase

assay was used in conjunction with the formic acid dehydrogenase assay to obtain the Michaelis-Menten plot (Figure 4-2a) as well as the Hanes-Woolf plot (Figure 4-2b). K_M and V_{max} were found to be 15.29 mM and 1.78 μmol min^{-1}, respectively.

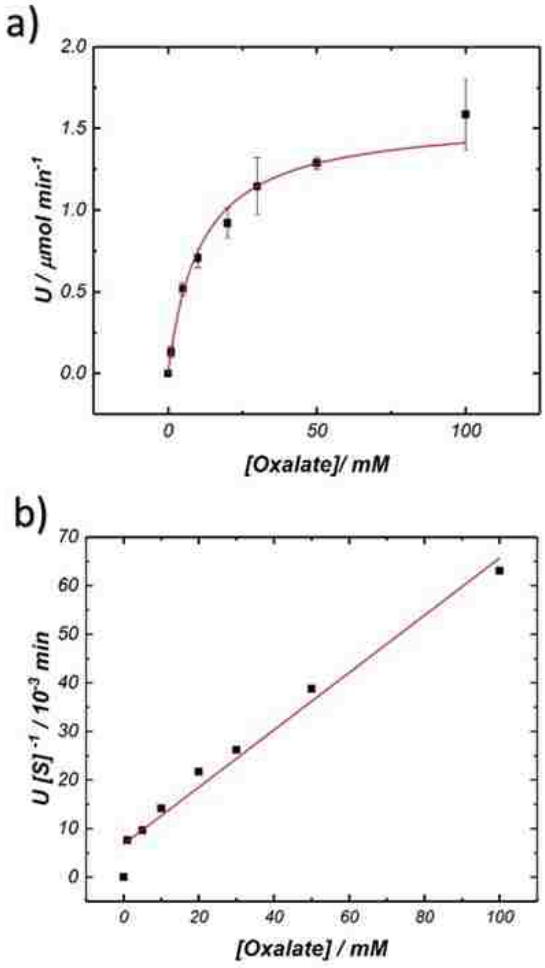

Figure 4- 2: a) Michaelis-Menten plot of the activity of OxDC in solution with oxalic acid. b) Hanes-Woolf plots derived from data in A). Kinetic measurements were performed at 25°C in 200 mM citric phosphate buffer, pH 4.0. All initial velocities were determined in triplicate.

Kinetics of Oxalate Decarboxylase on Multiwalled Carbon Nanotube Buckypaper

Michaelis-Menten and Hanes-Woolf plots were created for both physically adsorbed and tethered enzyme as shown in Figure 4-3, using the same procedure as the enzyme in solution. The K_M and V_{max} values were extrapolated from the Hanes-Woolf plots (Figure 4-3b). When the enzyme was immobilized on MWNT buckypaper through physical adsorption it was found that the Michaelis-Menten constant K_M, and maximum velocity, V_{max}, were 5.58 mM and 0.08 μmol min^{-1}, respectively. Next, OxDC was immobilized using the tether PBSE. The concentration of PBSE needed to be optimized for these sets of experiments because this either increases or decreases the kinetics of OxDC depending on if it was appropriately tethered to the buckypaper. It was determined that the optimized concentration of PBSE for immobilizing OxDC on MWNT buckypaper is 200 mM and K_M and V_{max} were determined as 4.69 mM and 0.19 μmol min^{-1}. Lower K_M indicates that the enzyme requires less substrate for the enzyme to consume to reach maximum velocity. These values are much lower than what was determined for the enzyme in solution. This could be attributed to the small immobilization efficiency or the structure change caused by the interaction with the surface. OxDC has a large hexameric structure which makes immobilization difficult [31], which is why different concentrations of PBSE were explored. If there was too little PBSE, the enzyme cannot be immobilized other than by physical adsorption, which lowers its kinetics. If there was too much PBSE, the enzyme may not be able to immobilize because the surface is too packed with the tether, which also lowers its kinetics. By finding the optimized concentration of PBSE on a simple system, such as

MWNT buckypaper, this method could then be extended to a more complex support. Table 4-1 lists the K_M and V_{max} determined for each of the concentrations that were explored from which the optimal concentration was determined.

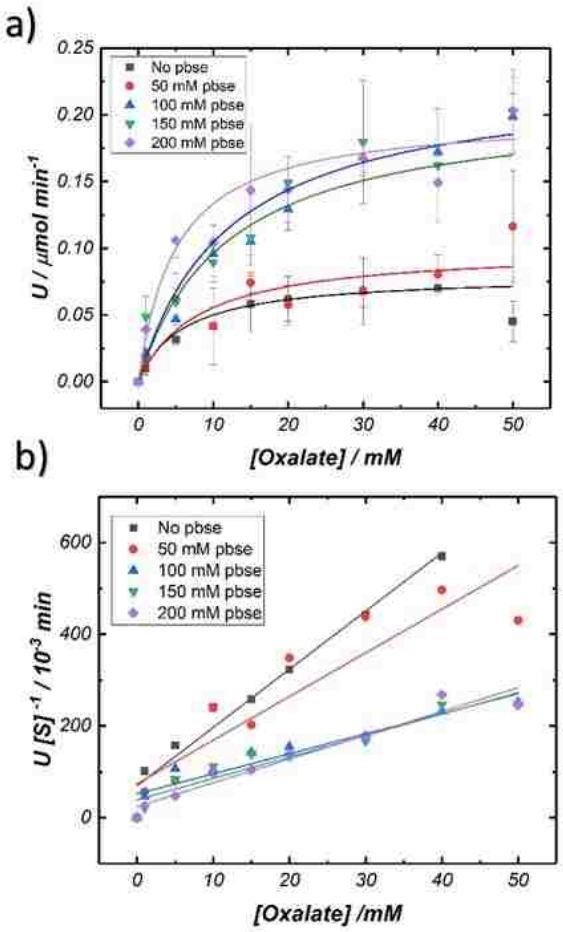

Figure 4- 3: a) Michaelis-Menten plot of the activity of OxDC immobilized on multiwall carbon nanotube buckypaper by physical adsorption (black), 50 mM (red), 100 mM (blue), 150 mM (green) and 200 mM PBSE (violet). b) Hanes-Woolf plots derived from data in a). Kinetic measurements were performed at 25°C in 200 mM citric phosphate buffer, pH 4.0. All initial velocities were determined in triplicates

Table 4- 1: Steady-state kinetic parameters obtained from the OxDC activity with oxalic acid on MWNT buckypaper. The kinetic parameters were calculated by non-linear regression analysis of experimental steady-state data.

PBSE concentration	K_m (mM)	V_m (nmol/min)
0 mM	5.58	0.08
50 mM	7.77	0.11
100 mM	11.89	0.23
150 mM	8.30	0.21
200 mM	4.69	0.19

Kinetics of Oxalate Decarboxylase on 3-Dimensional Graphene Nanosheets

The technique for immobilization of OxDC was then used and extended to a more complex support, 3D-GNS. Oxalic acid was converted by OxDC to formic acid and FDH oxidized formic acid to CO_2 (Scheme 4-2), while simultaneously NAD^+ is converted to NADH, which can be monitored at 340 nm using UV-Visible spectroscopy.

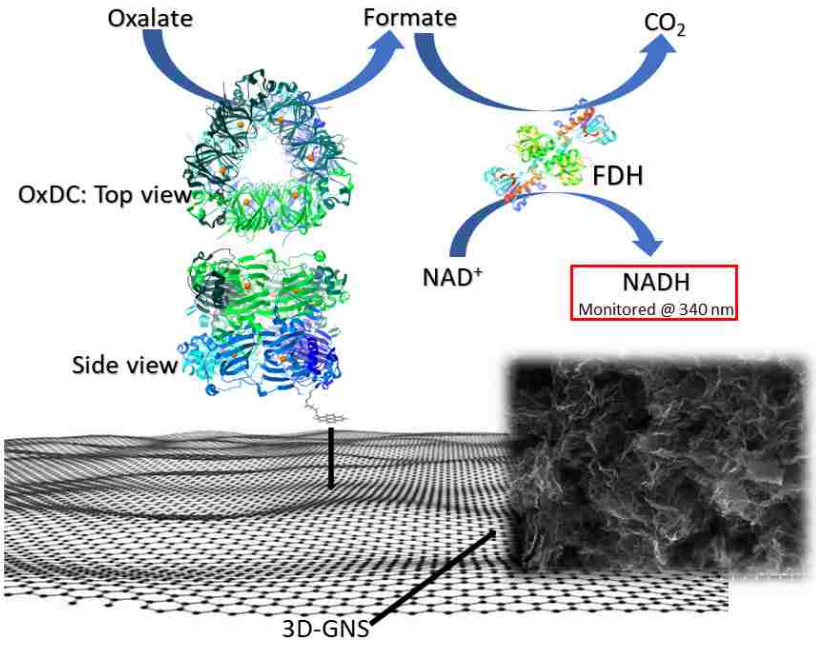

Scheme 4- 2: Reaction scheme of FDH assay used to determine immobilization of OxDC on 3D-GNS. OxDC converts oxalic acid to formic acid. FDH converts formic acid to CO_2 while the co-factor reaction of NAD^+ oxidizes to NADH and is visible at 340 nm.

This was done using the same tether, PBSE, and the same UV-Vis based FDH assay. Michaelis-Menten constants, K_M, and maximum velocity, V_{max}, for physically adsorbed OxDC as well as for tethered OxDC were determined by creating Michaelis-Menten and Hanes-Woolf plots (Figure 4-4). 3D-GNS have been developed and designed by our group in which the porosity and delivery of the substrates in carbonaceous materials are increased, which previously are used as supports for metal nanoparticles [32,33]. These supports are characterized with a network of porous channels within the graphene nanosheet matrix, which gives it a three-dimensional spatial arrangement and macroporous morphology. In addition, doping these supports with a transition metal or nitrogen can be used to introduce additional functionalities and modify the electronic properties of 3D-GNS supports, which can improve conductivity and facilitate charge transfer [17,34].

Several concentrations of PBSE were explored for this support because it was morphologically different than MWNT buckypaper. K_M and V_{max} values for physical adsorption of OxDC on 3D-GNS were determined as 1.70 mM and 0.05 μmol min^{-1}, respectively. Comparing these values to the values of OxDC that was physically adsorbed on MWNT buckypaper, K_M =5.58 mM and V_{max} = 0.08 μmol min^{-1}, we can conclude that smaller amounts of the substrate are needed to reach half of the maximal velocity for 3D-GNS.

However, the maximal velocity of OxDC on 3D-GNS was smaller than in the case of the enzyme immobilized on MWNT buckypaper. In both cases, the maximal velocity is much lower than compared to the maximal velocity of the enzyme in the solution. K_M and V_{max} for OxDC immobilized on 3D-GNS when using 150 mM PBSE as a tether, were determined as 0.60 mM and 0.07 μmol min^{-1}, respectively. Comparing these values to the values of physically adsorbed OxDC on 3D-GNS, K_M is three times smaller than it is used with the tether. This translates to the enzyme consuming less substrate to reach maximum velocity when it is tethered than it is for non-tethered. In addition, the maximal velocity of the enzyme increased from 0.05 to 0.07 μmol min^{-1}, indicating that the use of PBSE is beneficial both in the case of MWNT buckypaper and 3D-GNS. Now comparing the values obtained for OxDC immobilized on 3D-GNS and the values obtained for OxDC immobilized on MWNT buckypaper, K_M is smaller for 3D-GNS, and the maximal velocity decreased from 0.19 μmol min^{-1} to 0.07 μmol min^{-1}, indicating the enzyme immobilized on 3D-GN is less efficient then it is for MWNT buckypaper. This can be correlated to the differences in the morphological features between the two supports. Namely, 3D-GNS

have an intricate three-dimensional morphology, which is expected to decrease the interactions between the larger multimeric enzymatic systems and the carbonaceous support. Table 4-2 lists the values for K_M and V_{max} of the concentrations of PBSE that were explored for this support.

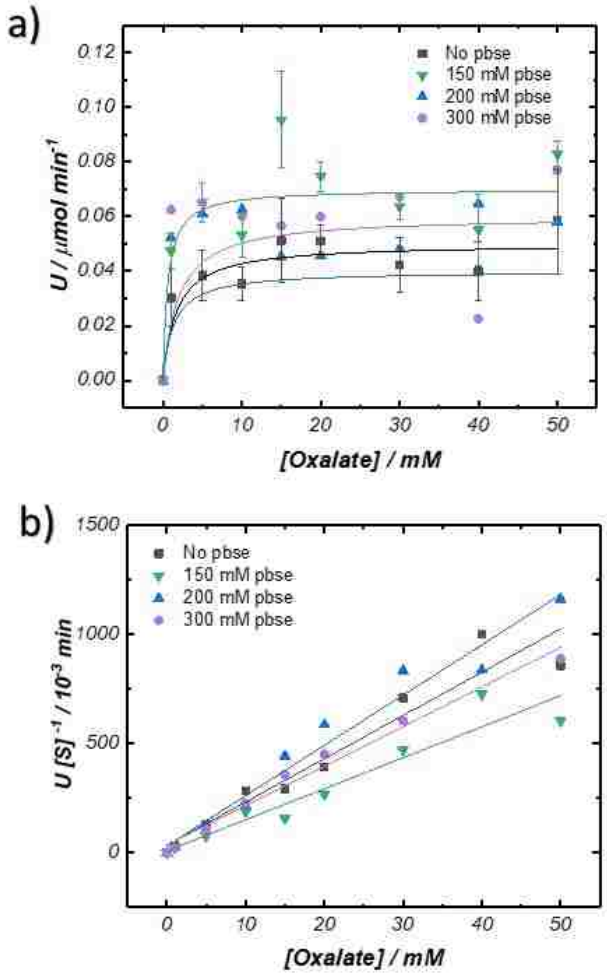

Figure 4- 4*:* a) Michaelis-Menten plot of the activity of OxDC immobilized on 3-dimensional graphene nanosheets by physical adsorption (black), 150 mM (green), 200 mM (blue), 300 mM and 300 mM PBSE (violet). b) Hanes-Woolf plots derived from data in a). Kinetic measurements were performed at 25°C in 200 mM citric phosphate buffer, pH 4.0. All initial velocities were determined in triplicates

Table 4- 2: Steady-state kinetic parameters obtained from the OxDC activity with oxalic acid on 3D-GNS. The kinetic parameters were calculated by non-linear regression analysis of experimental steady-state data.

PBSE concentration	K_m (mM)	V_m (nmol/min)
0 mM	1.70	0.05
150 mM	0.60	0.07
200 mM	1.34	0.04
300 mM	1.94	0.06

A procedure was designed and optimized to immobilize the large hexameric enzyme, oxalate decarboxylase from *Bacillus subtilis*, on multiwalled carbon nanotube buckypaper and 3D-Graphene nanosheets using 1-pyrenebutyric acid n-hydroxysuccinimide ester (PBSE) as a tethering agent. It was found that for this large hexameric enzyme, finding the optimal concentration was crucial for the enzymes performance by preventing disassociate of its subunits. The optimal amount of tether for the simple carbon support is 200 mM. OxDC was successfully immobilized on both a simple support, such as MWNT buckypaper, as well as a complex one; 3D-GNS, while retaining its functionality. The The optimal amount of tether for the simple carbon support is 150 mM.

Chapter 5

Design of Hybrid Enzymatic-Molecular Catalyst on 3D-GNS

The next objective was to incorporate the enzymatic catalyst with a molecular catalyst on the same platform to catalyze a two-step reaction. The molecular catalyst used is 2,2,6,6-(tetramethylpiperidin-1-yl)oxyl (TEMPO). It is a nitroxyl-radical containing compound and has many derivatives. It is capable of electrocatalytically oxidizing simple alcohols and amines in alkaline media [35]. 4-amino-TEMPO does not possess substrate limitations that enzymes do. The TEMPO used was modified by the Minteer group with a pyrene moiety so that it can be immobilized on the graphitic material.

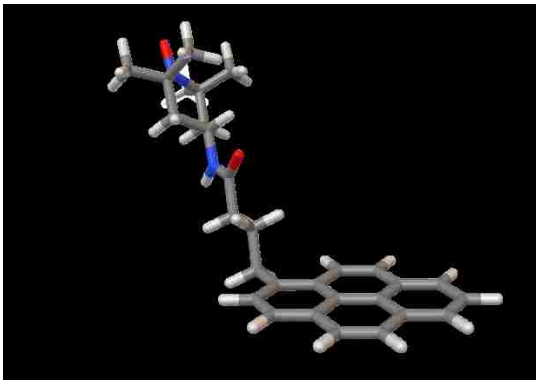

Figure 5- 1: Pyrene-TEMPO compound generated by Auto Dock Vina software.

This hybrid system will have its advantages and disadvantages. Enzymes are extremely fragile. They work in specific pH environments, temperatures and are specific to their substrates. However, organic and inorganic catalysts are less fragile, which promises to produce a more advanced system by its incorporation.

TEMPO is able to oxidize a wide range of alcohols and many substrates in the glycerol cascade that was designed and explored by the Minteer group [35]. The Minteer group also modified TEMPO with a pyrene base, which can be used to immobilize TEMPO in the same way the enzyme was immobilized. TEMPO modified with the pyrene moiety will be indicated as pyrene-TEMPO. Substrates of this family of molecular catalysts are primary and secondary alcohols, which means that TEMPO does not have much specificity and can oxidize most of the intermediates in the glycerol cascade. Scheme 5-1 shows the reaction scheme that is proposed for the two-step cascade. The two catalysts will be immobilized on the complex support 3D-GNS, as was successfully demonstrated for OxDC in the previous chapter. OxDC will convert oxalic acid to formic acid and formic acid will be further oxidized to CO_2 by pyrene-TEMPO. TEMPO is electrochemically active and the performance of the hybrid OxDC/pyrene-TEMPO catalyst will be studied by detecting the activity of TEMPO using electrochemical techniques.

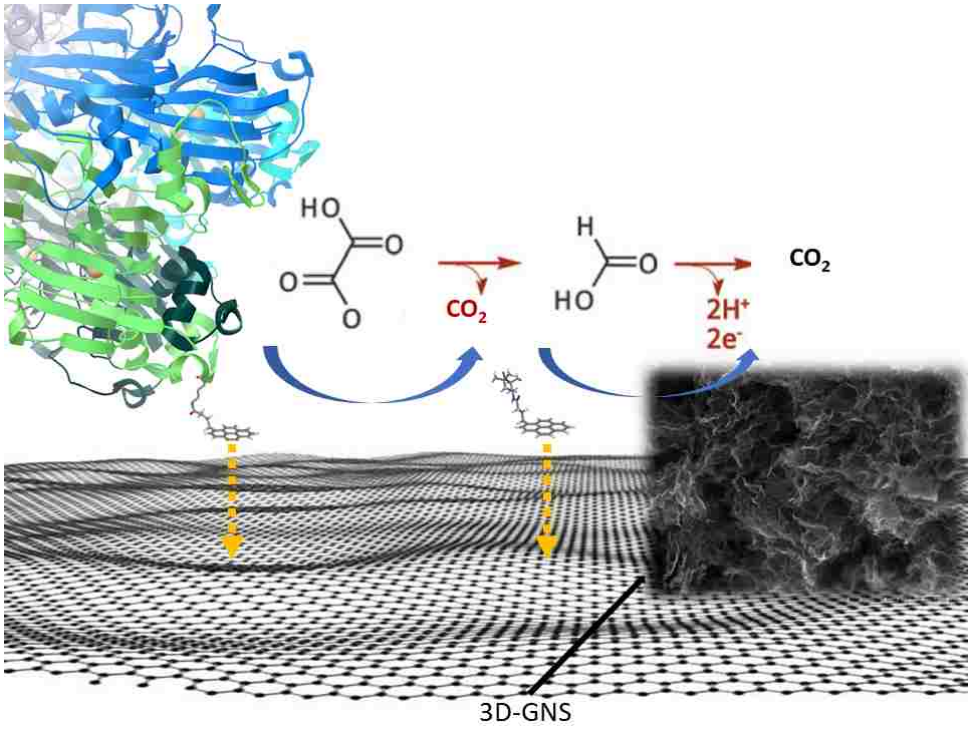

Scheme 5-1: OxDC tethered using PBSE and pyrene-TEMPO spatially organized on 3D-GNS. OxDC converts oxalic acid to formic acid and pyrene-TEMPO oxidizes formic acid to CO_2.

Pyrene-TEMPO Synthesis

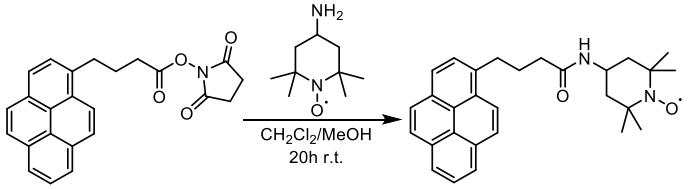

1.0 mmol PBSE was dissolved in CH_2Cl_2, which was then added to a stirred mixture of 1.1 mmol 4-amino-TEMPO in a mixture of 8:1 CH_2Cl_2/MeOH. This mixture was stirred for 20 hours at 25°C and after which it was concentrated under reduced pressure. The crude product was purified by a 5:1 hexane and ethyl acetate silica flash gel column chromatography. The solid product was obtained upon removal of solvent under reduced pressure (0.355 g, 80% yield). Prior to analysis, diphenylhydrazine was used to reduce the nitroxyl radical product to its corresponding hydroxylamine by NMR. ^{1}H-NMR (300 MHz,

$CDCl_3$): δ 8.30 (d, 1H), 8.16 – 8.10 (m, 4H), 8.00 (t, 1H), 7.88 (d, 1H), 5.04 (s, 1H), 4.17 (s, 1H), 3.40 (s, 2H), 2.22 (s, 4H), 1.80 (dd, 2H), 1.19 (s, 6H), 1.15 (s, 6H).

Bimodal Electrode Preparation

Pyrene-TEMPO/3D-GNS was prepared in a vial by combining 40 µL of base ink with 8 µL of 100 mM solution of pyrene-TEMPO dissolved in acetone, and 2 µL of citric phosphate buffer. The base ink was made by combining 5 mg of 3D-GNS in 925 µL of DI and 75 µL tetrabutylammonium bromide Nafion (TBAB). 5 mg of TBAB was sonicated in 80 µL of acetone for 10 minutes. 10 µL of the pyrene-TEMPO/3D-GNS was then drop-casted onto a glassy carbon electrode and dried.

OxDC/3D-GNS was prepared in a vial by combining 40 µL of base ink, 8 µL of the tether (150 mM solution of PBSE dissolved in acetone), and 2 µL of OxDC from *Bacillus subtilis* with the concentration of 2.3 mg/mL. 10 µL of the OxDC/3D-GNS was then drop-casted onto a glassy carbon electrode and dried. The electrodes were kept at 4°C for 16-18 hours to cure before the electrochemical and UV-VIS measurements. Before performing experiments, electrodes were washed in citric phosphate buffer to remove any enzyme that was not immobilized.

To make OxDC/pyrene-TEMPO/3D-GNS electrodes, 25 µL of pyrene-TEMPO/3D-GNS and 25 µL of OxDC/3D-GNS were combined in a separate vial. 10 µL of the vial content was then drop-casted onto a glassy carbon electrode and dried. The electrodes were kept at

4°C for 16-18 hours to cure and then washed with citric acid buffer to remove any enzyme or pyrene-TEMPO that was not immobilized. The electrodes were then immersed in 100 mM oxalic acid or 100 mM formic acid for electrochemical experiments.

Bimodal Electrochemical Measurements

Electrochemical experiments were performed using a three-electrode half-cell with the Ag/AgCl electrode as a reference electrode and a platinum wire as the counter electrode. A glassy carbon electrode on which the prepared ink was drop-casted was used as the working electrode. The control experiments were performed using a citric phosphate buffer, which consisted of 0.1 M citric acid and 0.2 M sodium phosphate dibasic at pH 5.2, which was purged with N_2. All the cyclic voltammogram (CV) were obtained in a potential window between 0 and 0.85 V at a scan rate of 10 mV/s. After the control curves were obtained, 100 mM of a substrate (oxalic acid or formic acid) was introduced and the cyclic voltammograms were recorded using the same potential range and the same scan rate. The cyclic voltammograms reported in the manuscript show the third scan, which corresponds to the steady state. All electrochemical experiments were done in triplicates to confirm their reproducibility.

Activity of Molecular Catalyst

To demonstrate the two-step cascade of the conversion of oxalic acid to formic acid to CO_2, pyrene-TEMPO was first explored to determine if it could be immobilized and function

after immobilization. Cyclic voltammograms of pyrene-TEMPO on 3D-GNS in CPB, pH 5.2, (black) and 100 mM formic acid (red) in Frigure 5-2a shows that pyrene-TEMPO is active towards formic. The pH 5.2 was chosen because this is the pH that overlaps for the two catalysts activity [19]. The maximum current was determined as 674.4 ± 20.9 μA cm^{-2} for the potential window of 0 to 0.8 V, which was calculated by taking the difference of the current obtained from the substrate and in the buffer at U = 0.8V. The onset potential was 0.608 V and was determined by using Eq 7. It was the potential at which the current increased to 10 times the standard deviation of the capacitive current.

$$Onset\ potential = U\ (I\ capacitive + 10 * average\ (stdev) \quad (8)$$

The measured onset potential for pyrene-TEMPO in formic acid was in agreement with the onset potential for the oxidation of formic acid by 4-amino-TEMPO determined in previous work as 0.668 V vs. SCE [19]. The activity of formic acid was also tested on 3D-GNS alone and showed that 3D-GNS has no activity towards formic acid (Figure 5-2b). This also confirms that pyrene-TEMPO is active while immobilized onto 3D-GNS and that the observed activity was not due to the 3D-GNS. Therefore, we can conclude that pyrene-TEMPO can be successfully immobilized on 3D-GNS.

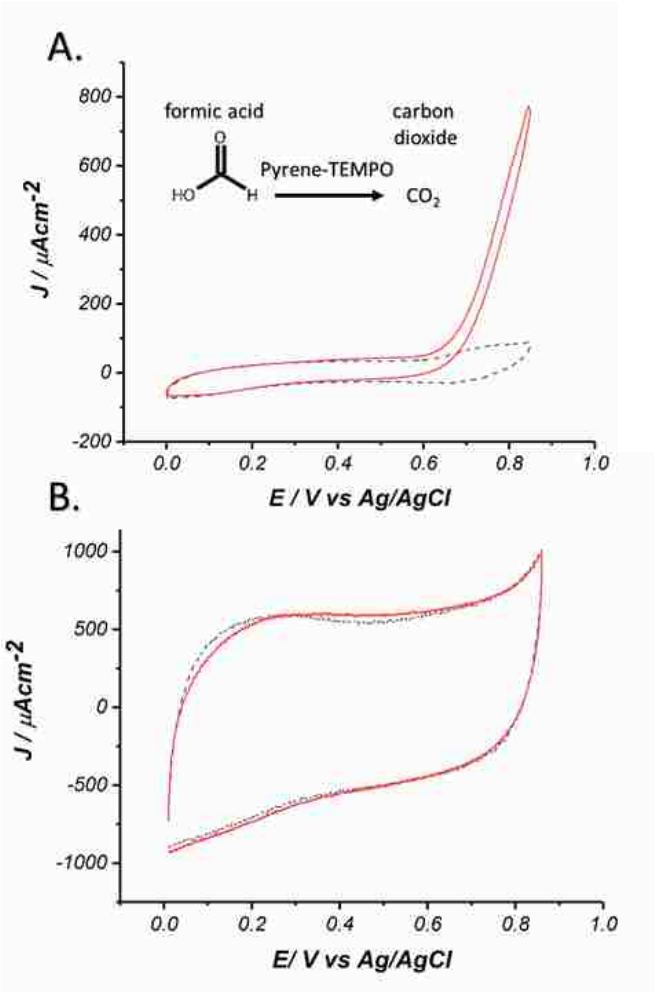

Figure 5- 2: a) CV of pyrene-TEMPO/3D-GNS in 0.1 M citric phosphate buffer (black) and 100 mM formic acid (red). b) CV of 3D-GNS in the 0.1 M citric acid buffer (black) and 100 mM formic acid (red). Experiments were performed at pH 5.2 and 25°C with a scan rate of 10 mV/s.

Hybrid Enzymatic-Molecular Catalyst on 3D-GNS

To go forward with this two-step cascade, OxDC and pyrene-TEMPO were also tested for each substrate in the two-step cascade individually. Pyrene-TEMPO on 3D-GNS was tested in oxalic acid and formic acid as well as OxDC on 3D-GNS in oxalic acid and formic acid. The results show that pyrene-TEMPO has minimal activity for oxalic acid (Figure 5-

3). The maximal current density and onset potential was 116.6 ± 77.5 μA cm^{-2} and 0.605 V. These results show that the observed activity of the hybrid system is not due to the activity of pyrene-TEMPO towards oxalic acid.

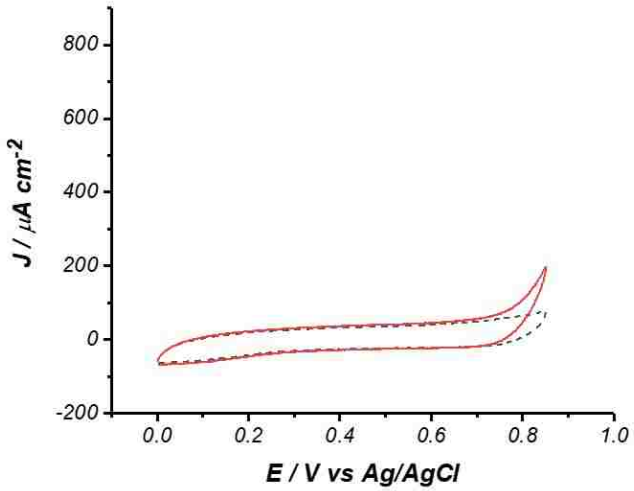

Figure 5- 3: CV of pyrene-TEMPO/3D-GNS in 0.1 M citric phosphate buffer (black) and 100 mM oxalic acid (red). All measurements were performed at pH 5.2 and 25°C with a scan rate of 10 mV/s.

Several other control studies were performed to confirm the validity of the two-step cascade. OxDC/3D-GNS in oxalic acid showed minimal activity of 132.3 ± 14.8 μA cm^{-2} and an onset potential of 0.617 V (Figure 5-4). Again, from these results, we can conclude that the observed activity of the hybrid catalyst was not due to OxDC in oxalic acid.

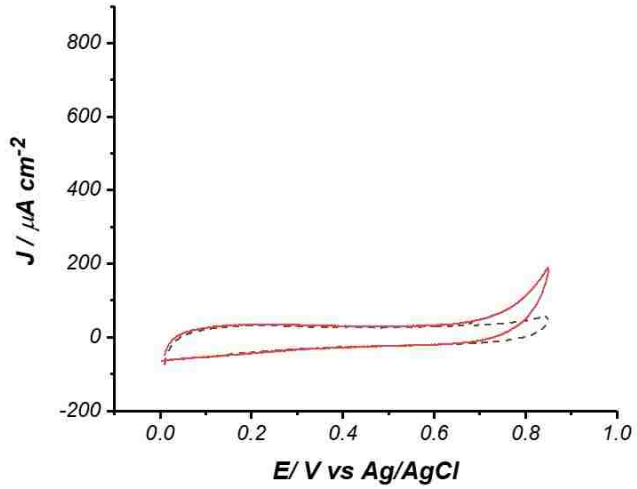

Figure 5- 4: CV of OxDC/3D-GNS in 0.1 M citric phosphate buffer (black) and 100 mM oxalic acid (red). All measurements were performed at pH 5.2 and 25°C with a scan rate of 10 mV/s.

Furthermore, there was no activity when formic acid is introduced to OxDC/3D-GNS, which suggests that OxDC immobilized on 3D-GNS is not active towards formic acid (Figure 5-5). These control experiments show that the current observed with the hybrid catalyst was not due OxDC in the presence of oxalic acid or formic acid.

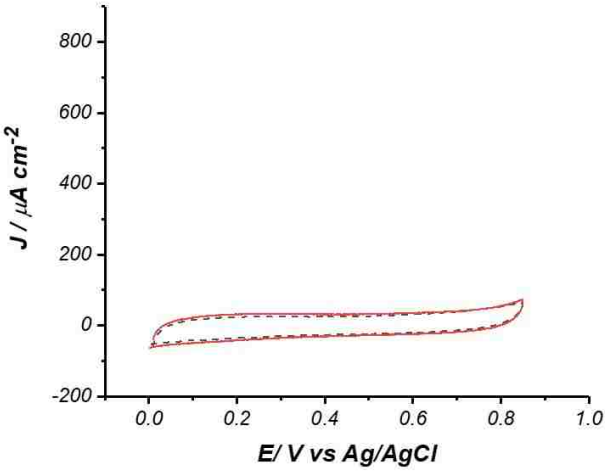

Figure 5- 5: OxDC/3D-GNS in 0.1 M citric phosphate buffer (black) and 100 mM formic acid (red). All measurements were performed at pH 5.2 and 25°C with a scan rate of 10 mV/s.

However, the CVs in Figure 5-6 show that there is activity of 3D-GNS in oxalic acid which can be attributed to the impurities in the support. The activity is greatly suppressed in the presence of the immobilized enzyme, which is supported by CVs in Figure 5-4. This shows that the small activity observed with OxDC in oxalic acid was not due to OxDC but probably the ability of 3D-GNS to oxidize oxalic acid. The activity of OxDC/3D-GNS in oxalic acid was still small compared to the activity of the OxDC/pyrene-TEMPO hybrid in oxalic acid, which means that the current observed with the hybrid catalyst provides evidence for a two-step cascade reaction and is not due to the oxidation of oxalic acid by OxDC/3D-GNS.

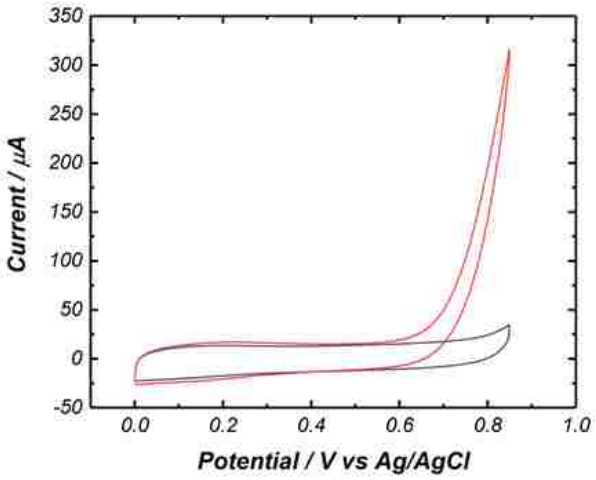

Figure 5- 6: CV of 3D-GNS in 0.1 M citric phosphate buffer (black) and 100 mM oxalic acid (red). All measurements were performed at pH 5.2 at 25°C with a scan rate of 10 mV/s.

Finally, the hybrid system of OxDC/pyrene-TEMPO/3D-GNS shows a maximal current of 361.6 ± 88.6 µA cm^{-2} and onset potential of 0.592 V (Figure 5-7). This confirms that the two-step cascade, first of all, was working, and second, the observed activity was due

pyrene-TEMPO in the presence of formic acid, which was converted from oxalic acid by the enzyme.

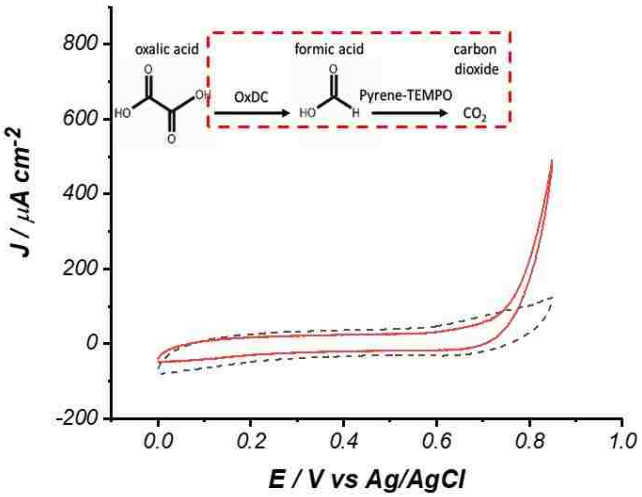

Figure 5- 7: CV of OxDC/pyrene-TEMPO/3D-GNS in 0.1 M citric phosphate buffer (black) and 100 mM oxalic acid (red). All measurements were performed at pH 5.2 and 25°C with a scan rate of 10 mV/s.

Electrochemical techniques were used to demonstrate that two catalysts of two different modalities, an enzymatic and molecular catalysts, can be immobilized and co-localized on 3D-GNS. As confirmed by the means of electrochemistry, this hybrid system is able to catalyze two-subsequent reactions. The support used has also been proven to be a superior support for the incorporation of metallic nanoparticles as catalytic sites. This work, therefore provides a path for designing more complex assemblies that would contain any combination of an enzymatic, molecular, and inorganic catalyst. This chapter has been completed and a paper was prepared combining this chapter and chapter 4 and submitted to Electrochemical Acta. Work in chapter 6 incorporate a third catalyst supported on the 3D-GNS to complete a multi-step cascade reaction.

Chapter 6

Incorporation of Three Catalysts of Three Different Modalities

In the previous work by Atanassov group, , the enzyme, OxDC, has been co-localized with PdNP decorated on 3D-GNS. This was successfully accomplished at pH 5.2 in 0.1 M citric phosphate buffer at room temperature. The enzyme converts oxalic acid to formic acid and PdNP oxidized formic acid to CO_2. However, the enzyme immobilization was not characterized by any techniques to confirm its immobilization nor were the kinetics optimized. In the previous chapters, it was also shown that the enzyme could be successfully co-localized with the molecular catalyst, pyrene-TEMPO, on 3D-GNS. The immobilization of the enzyme and characterization of the two-step cascade reaction discussed in detail in the previous chapters.

The objective in this task were to incorporate all three catalysts on the same support, co-locally, and create a functional hybrid catalyst (Scheme 6-1) that can convert glyoxalic acid to CO_2 protons and electrons. There was observed activity in the previous hybrid enzymatic-molecular catalyst, however, in this part of the proposal, the aim is not only to spatially organize all three catalysts of three different modalities to catalyze a multi-step cascade reaction but to also achieve efficiency. TEMPO functions in more basic conditions while the enzyme naturally operates in more acid conditions. Previous studies by Minteer group were done, without manipulation of the catalysts, to identify an overlapping pH = 5.2. However, in this part of the proposal pH was set to 6.2. Namely, the molecular catalyst

is more active towards glyoxalic acid at higher pHs and a mutant of OxDC, which will be used at pH 6.2, had to be developed. In addition, gold nanoparticles will replace the palladium nanoparticles because gold nanoparticles are more selective for the substrates in the glyoxalic acid cascade. The first reaction will be catalyzed by the molecular catalyst, TEMPO, which will oxidize glyoxalic acid to oxalic acid. The second reaction will be performed by the enzymatic catalyst, OxDC, which will convert oxalic acid to formic acid. Finally, the last reaction will be catalyzed by the inorganic catalyst, Au, which will oxidize formic acid to CO_2. All catalysts will be co-localized on the same support.

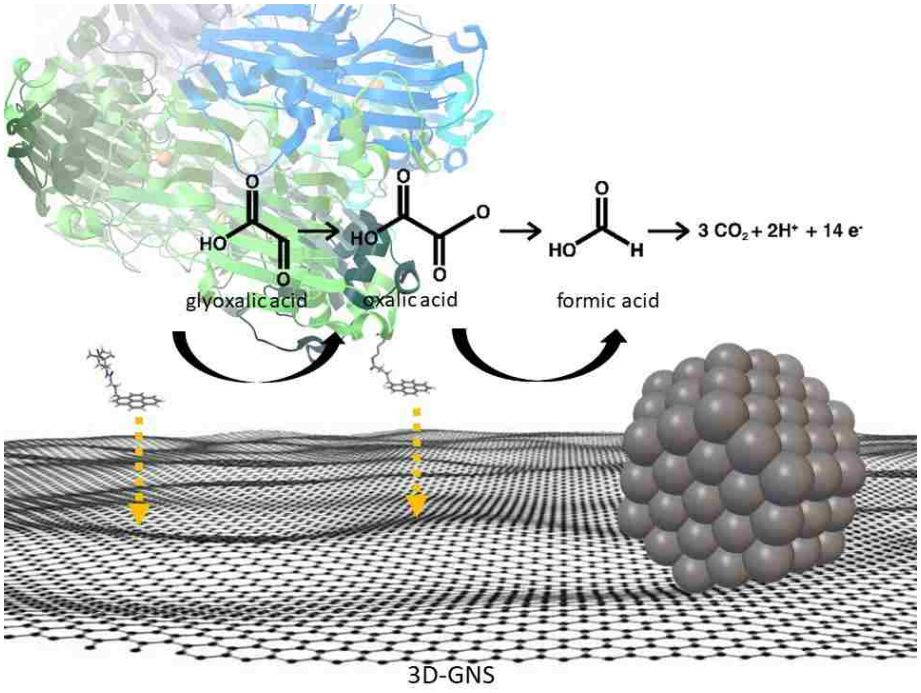

Scheme 6- 1: OxDC tethered by PBSE and pyrene-TEMPO spatially organized on 3D-GNS that is decorated with PdNP. Pyrene-TEMPO oxidizes glyoxalic acid to oxalic acid. OxDC converts oxalic acid to formic acid and the PdNP oxidize formic acid to CO_2.

Au colloid synthesis using polyol method

The gold colloid was prepared using the polyol method [36,37]. 60 mL of ethylene glycol was dissolved in 4.2 g of PVP stirred at room temperature (which yields 5.1wt.% PVP: ethylene glycol). The solution was heated to 120°C. 30 mg of gold (III) chloride hydrate ($HAuCl_4 \cdot aq$) was dissolved in 10 mL of ethylene glycol at room temperature. This was added to the PVP-ethylene glycol solution and proceeded for 2 hours.

Au decorated on 3D-GNS

The gold colloid solution was added to 3D-GNS (to yield 20wt.% loading of Au:carbon) then the pH was adjusted, using sulfuric acid, to pH=2.5. After, the solution was cover and stirred for 22 hours.

Ink Preparation for Hybrid Catalyst

Au//3D-GNS was prepared in a vial by combining 40 µL of base ink with 10 µL of citric phosphate buffer (pH 6.2). The base ink was made by combining 5 mg of 3D-GNS in 925 µL and 75 µL TBAN Nafion. 5 mg of TBAB was sonicated in 80 µL of acetone for 10 minutes. 3 µL of the Pd/3D-GNS was then drop-casted onto a glassy carbon electrode and dried.

To make $OxDC_{MUT}$/Au/3D-GNS, 40 µL of solution A, 8 µL of solutions B (150 mM solution of PBSE sonicated in acetone 10 minutes) and 2 µL of 2.3 mg/mL $OxDC_{MUT}$ were combined in a vial.

To make pyrene-TEMPO/Au/3D-GNS, 40 µL of solution A was combined with 10 µL of (150 mM solution of pyrene-TEMPO dissolved in acetone).

Electrode Preparation for Hybrid Catalyst

To make $OxDC_{MUT}$/pyrene-TEMPO/Au/3D-GNS electrodes, 25 µL of pyrene-TEMPO/Au/3D-GNS and 25 µL of $OxDC_{MUT}$/Au/3D-GNS were first combined in individual vials and then combined into one vial after 10 minutes. 3 µL of the vial content was then drop-casted onto a glassy carbon electrode and dried. The electrodes were kept at 4°C for 16-18 hours to cure and then washed with citric acid buffer to remove non-immobilized components. The electrodes were then immersed in 100 mM glyoxalic acid for electrochemical experiments.

Design and Engineering of Hybrid Catalyst -- Molecular Catalyst

In this part of the proposal, the focus was to analyze each step of the cascade with the desired catalysts to ensure the presence of a multi-step reaction. The multi-step cascade reaction begins with the molecular catalyst, TEMPO, which will oxidize glyoxalic acid to oxalic acid. It was previously shown that pyrene-TEMPO/3D-GNS is active towards

formic acid (Figure 5-2a) and shows minimal activity towards oxalic acid (Figure 5-3). Cyclic voltammograms were taken of pyrene-TEMPO/3D-GNS in glyoxlaic acid (0.1 M CPB pH=6.2) to provide evidence that in the first part of the cascade, glyoxalic acid will be oxidized to the next substrate (Figure 6-2). The pH was changed from 5.2 to 6.2 because 1) the molecular catalysts was more active for glyoxalic acid at a higher pH and 2) the mutant enzyme was engineered to function at pH as high as 6.2

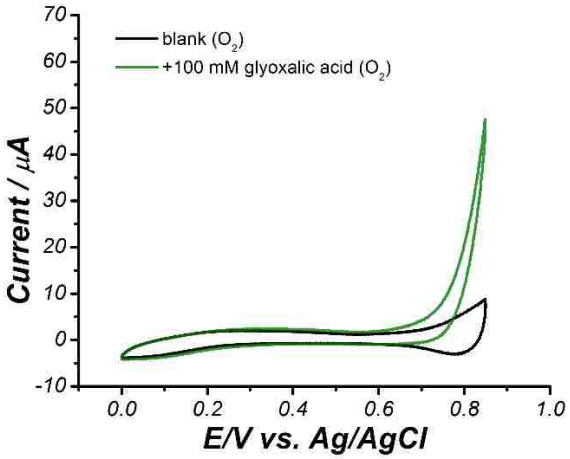

Figure 6- 1: CV of pyrene-TEMPO/3D-GNS in 100 mM glyoxalic acid (0.1 M CPB pH=6.2 at 25°C).

The CV in Figure 6-1 shows that pyrene-TEMPO can oxidize glyoxalic acid at higher pH. This suggests that the activity of pyrene-TEMPO in the presence of glyoxalic acid will not be overtaken by the oxidation of formic acid by pyrene-TEMPO in the presence of formic acid.

Design and Engineering of Hybrid Catalyst -- Enzymatic Catalyst

The second reaction in the cascade will be catalyzed by an enzymatic catalyst, which will convert oxalic acid to formic acid. The overlapping pH for TEMPO and $OxDC_{WT}$ (wild

type) was pH 5.2. However, the optimal pH for $OxDC_{WT}$ was approximately pH = 4. TEMPO and its derivatives perform better at higher pHs. The Minteer group have been working towards an enzyme that functions at a higher pH to be able to gain the maximum activity of TEMPO electrochemically. The overlapping pH for the engineered enzymes and the molecular catalyst was found to be pH=6.2. Enzyme 1: OxDC mutant 3-3-8 E4, has one mutation, R66Q, concentration 21 mg/mL, and specific activity of 20 U/mg. Enzyme 2: OxDC mutant 3-3-3 F3 has two mutations, I91T and E147D, 38 mg/mL, and specific activity of 14 U/mg. These two enzymes were incorporated in the hybrid-molecular-enzymatic two-step cascade and tested for their ability to convert oxalic acid to formic acid. The maximum currents due to oxidation of formic acid by pyrene-TEMPO, were determined as 16 μA, 7.3 μA, and 1.3 μA for the hybrid containing $OxDC_{WT}$, OxDC 3-3-8-E4, and OxDC 3-3-3-F3, respectively. To determine which mutant enzyme to move forward with, CVs of the mutant enzyme-molecular catalyst were compared to the performance of the wild type enzyme-molecular catalyst at pH=5.2 (Figure 6-2a), which was studied in the previous chapter. The objective was to determine if the enzymes can function at the proposed higher pH (pH=6.2) not enhance their function. These results, im Figure 6, show that both proposed enzymes OxDC 3-3-8-E4 (Figure 6-2b) and OxDC 3-3-3-F3 (Figure 6-2c) can convert oxalic acid to formic acid at pH 6.2. The currents observed are due to the subsequent oxidation of formic acid on pyrene-TEMPO because the enzyme is not electrochemically active. Therefore, it can be concluded that these two enzymes can be used towards the synthetic cascade system at pH 6.2.

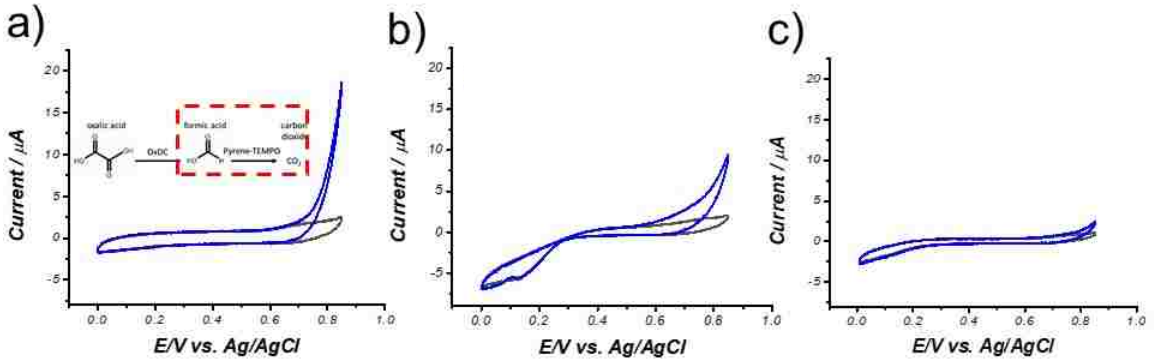

Figure 6- 2: CV of the hybrid enzymatic-molecular system in citric phosphate buffer pH = 5.2 (black) and 100 mM oxalic acid (blue) purged in O_2 for a) $OxDC_{WT}$ (pH=5.2), b) OxDC 3-3-8-E4 (pH=6.2), c) OxDC 3-3-3-F3 (pH=6.2).

Table 6-1 reviews the currents and onset potentials for the three possible OxDC that could still function in this system. Maximum current values for the hybrid catalyst containing OxDC 3-3-8-E4 and OxDC 3-3-3-F3 were determined to be 7.3 µA and 1.3 µA, respectively. The results show that either of the two enzyme mutants would perform the second reaction in this sophisticated cascade at pH=6.2, however, to introduce some system efficiency, OxDC 3-3-8-E4 was chosen for the further work on of designing the hybrid catalyst for the multi-step cascade system.

Table 6- 1: Electrocatalytic screening of OxDC mutants in oxalic acid. Catalytic activity was determined by comparison of cyclic voltammograms in the presence and absence of 0.1 M oxalic acid using 0.1 M CPB, pH = 6.2, at 25 °C.

Enzyme	$OxDC_{WT}$	$OxDC_1$ (3-3-8-E4)	$OxDC_2$ (3-3-3-F3)
Maximum Current [µA]	16	7.3	1.3
Onset Potential [V]	0.592	0.559	0.598

Design and Engineering of Hybrid Catalyst -- Metallic Catalyst

The third reaction in which of formic acid is oxidized to CO_2 can be performed by the palladium nanoparticles. These nanoparticles are decorated on 3D-GNS at a 20wt.% loading of Pd:carbon[38]. Each nanoparticle was 5-7 nm in diameter, which is almost half the size of the OxDC enzyme (Figure 6-3).

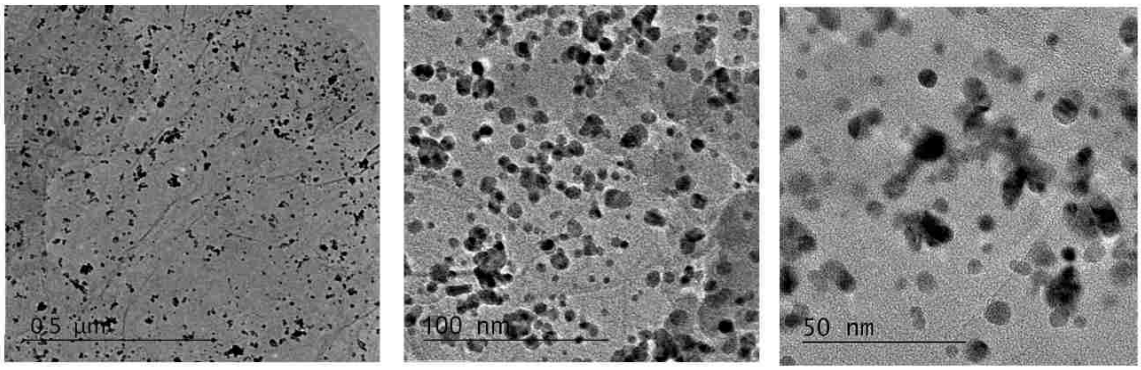

Figure 6- 3: TEM micrographs of Pd nanoparticles deposited on thermally reduced 3D-Graphene nanosheets.

The objective of this part of the cascade was to test if the metallic catalyst was active and selective towards for formic acid oxidation. The activity of Pd/3D-GNS towards the three substrates in the cascade (glyoxalic acid, oxalic acid, and formic acid) was studied by collecting voltammograms. Figure 6-4a shows that palladium was most active toward formic acid with low onset potential. However, the results also show tha Pd/3D-GNS is also active for glyoxalic and oxalic acid (Figure 6b-c). This implies that the catalyst would overtake the whole cascade without producing a multi-step cascade reaction performed by multiple catalysts. In addition, when the activity of pallidum towards glyoxalic acid was compared to the activity of the molecular catalyst (Figure 6-1) in glyoxalic acid, palladium

was more active toward glyoxalic acid than the molecular catalyst. Attempts were made to poisoning the catalyst to improve selectivity, but this strategy was not successful. In most cases, changing to another metal would be less favorable, but in our case this wa proven to be a more viable approach.

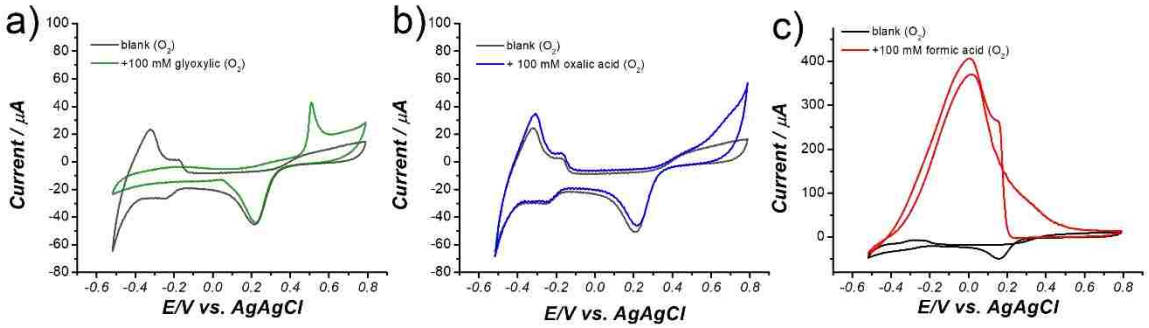

Figure 6- 4: CV of Pd/3D-GNS in 100 mM a) glyoxalic acid b) oxalic acid and c) formic acid in 0.1 M CPB pH=6.2 at 25°C in O_2.

To avoid the entire cascade to be overtaken by palladium, gold was proposed as the new metallic catalyst. Gold binds all oxygenated intermediates involved in the alcohols oxidation much weaker than Pd, resulting in reduced performances [39,40,41,42]. A gold colloid solution was made using 5.1wt.% PVP: ethylene glycol as the surfactant so the nanoparticles would be supported in solution without their structure being destroyed. The reaction took place at 150°C for 2 hours. To characterize the Au nanoparticles, TEM micrographs were taken using a JOEL model at 60 K. Figure 6-5 shows on average, the size of the gold nanoparticle was much larger than that of the palladium nanoparticles.

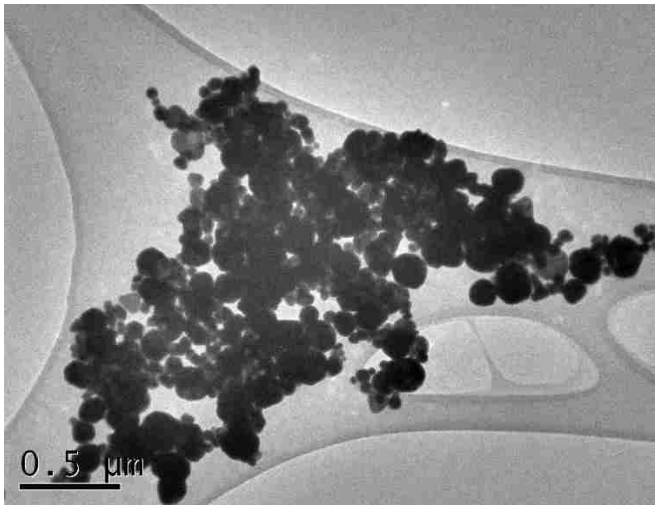

Figure 6- 5: TEM micrographs of Au nanoparticles from colloid solution.

Cyclic voltammograms in each substrate of the multi-step cascade were obtained to determine the activity of the Au nanoparticles towards each substrate. Figure 6-6a shows that gold inhibits the oxidation of glyoxalic acid. Observably, there was almost no current difference between the blank and the substrate. The objective was to have a metallic catalyst that was more selective for the substrates in the cascade rather than it being more active for formic acid.

As seen in a previous chapter, the activity of the Au/3D-GNS for the oxidation of oxalic acid (Figure 6-5b) is identical to the activity of the carbon support for the oxidation of oxalic acid (Figure 5-6). This suggests, that at high potentials, the 3D-GNS also contributes to the oxidation of oxalic acid. This was also the case for other tested carbon supports (Appendix A3).

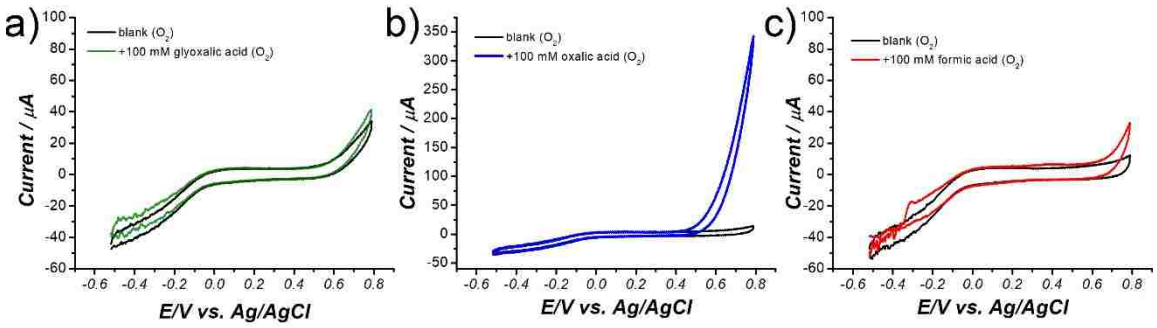

Figure 6- 6: CV of Au/3D-GNS in 100 mM a) glyoxalic acid b) oxalic acid and c) formic acid in 0.1 M CPB pH=6.2 at 25°C in O_2.

Figure 6-6c further shoes that gold was active for formic acid; however, the onset potential was approximately 0.2 V vs. Ag/AgCl, and the peak current for the oxidation of formic acid oxidation was surprisingly low. This could be explained by the contamination of the gold surface due to the surfactant (PVP). For that reason, the amount of surfactant was further investigated and optimized.

Different Au colloid solutions have been deposited on 3D-GNS, varying the amount of surfactant in the colloid solution. Two amounts of surfactants have been tested, 1wt.% (Figure 6-7a) and 4.8wt.% (Figure 6-7b). As prepared Au/3D-GNS were then tested towards the oxidation of formic acid. Figure 6-7 shows that as the decrease in the amount of surfactant increases the peak current and that the 1wt.% of surfactant produced Au/3D-GNS with the highest activity for formic acid oxidation. Not enough surfactant in the colloid solution will cause the nanoparticles to collapse resulting in little or few nanoparticles.

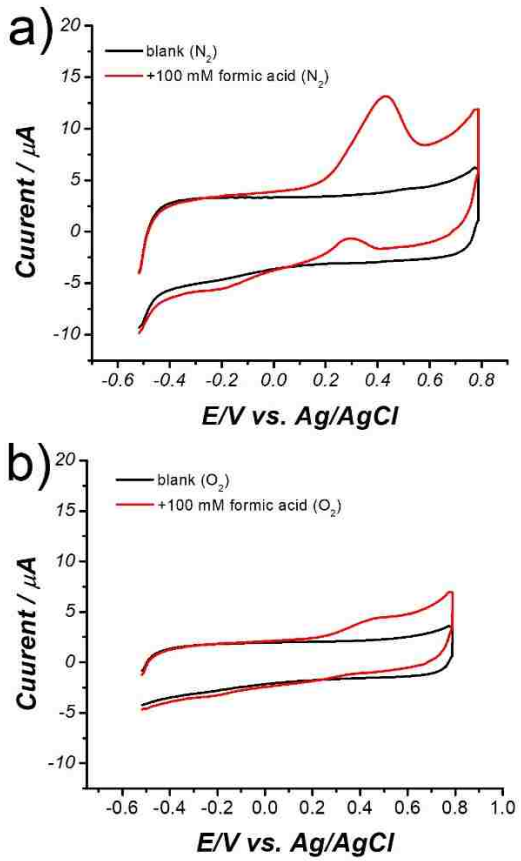

Figure 6- 7: CV of Au/3D-GNS in 100 mM formic acid (0.1 M CPB pH=6.2 at 25°C in O_2) using a) 1 wt.% PVP and b) 4.8 wt.% PVP.

Design and Engineering of Hybrid Catalyst

Half of the cascade was tested to determine the impact of the enzyme: the activity of the $OxDC_1$/Au/3D-GNS (Figure 6-8b) and $OxDC_1$/Pd/3D-GNS (Figure 6-8c) was tested in the presence of oxalic acid. When comparing these with their base components we find that the enzyme does not have an impact on the electrochemistry of the cascade. For example, when comparing $OxDC_1$/Au/3D-GNS (Figure 6-8b) with Au/3D-GNS (Figure 6-6b), in the presence of oxalic acid, the peak current of both systems was approximately the same. The same comparison can be made for the palladium based system.

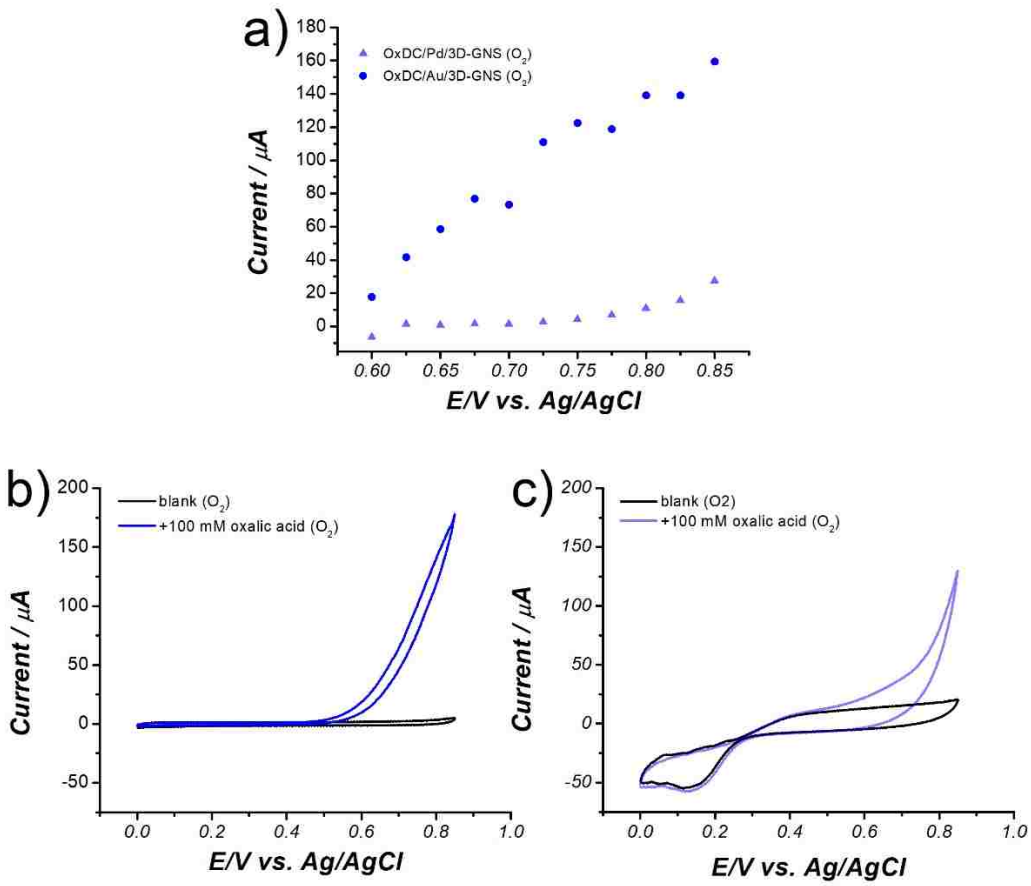

Figure 6- 8: a) activity curve of hybrid catalyst in the presence of 100 mM oxalic acid for $OxDC_1$/Au/3D-GNS (circle) and $OxDC_1$/Pd/3D-GNS (triangle). CVs for b) $OxDC_1$/Au/3D-GNS and c) $OxDC_1$/Pd/3D-GNS in 100 mM oxalic acid (blue) buffered with 0.1 M CPB pH=6.2 in O_2.

The result is both expected and problematic. The enzyme is not electrochemically active; hence the signal is due to the metallic catalyst OxDC should convert oxalic acid to formic acid, which can be further oxidized by Au and Pd. The fact that the onset potential is not lower, indicated that we are observing oxidation of oxalic acid by the metal nanoparticles while as we should see the oxidation of the formic acid by the nanoparticles. One explanation for this is that there was not enough reaction time for the enzyme to convert oxalic acid to formic acid for further oxidation. A second reason was that the Au and Pd nanoparticles are either not as non-accessible because covered by the enzyme or partly

poisoned by the PVP (for Au). The latter may be the more likely case, as it was shown in a previous chapter when the enzyme was immobilized, in the presence of oxalic acid, the signal suppressed (Figure 5-4). The carbon support can also oxidize oxalic acid which results in large current. With the optimized amount of immobilized enzyme, the support cannot oxidize oxalic acid has previously been seen. However, in the case of Au and Pd, there was a large peak current even with the enzyme immobilized and this could be due to the fact that the previous optimized tether amount was no longer relevant because of the presence of gold in the system taking up the surface area of the 3D-GNS. Also, too much tether on the surface causes the decrease in activity of the enzyme, as discussed in Chapter 4.

To reiterate, the enzyme does not have an impact on the signal in the CV studies as it is not electrochemically active. OxDC therefore converts oxalic acid to formic acid without exchanging electrons with the electrode. This can be confirmed by testing an electrochemically active catalyst alone and adding the enzyme (Figure 6-9). Pyrene-TEMPO alone on 3D-GNS compared to pyrene-TEMPO with $OxDC_1$/3D-GNS shows no difference in activity in the presence of glyoxalic acid. The signal in the separate graphs are almost identical.

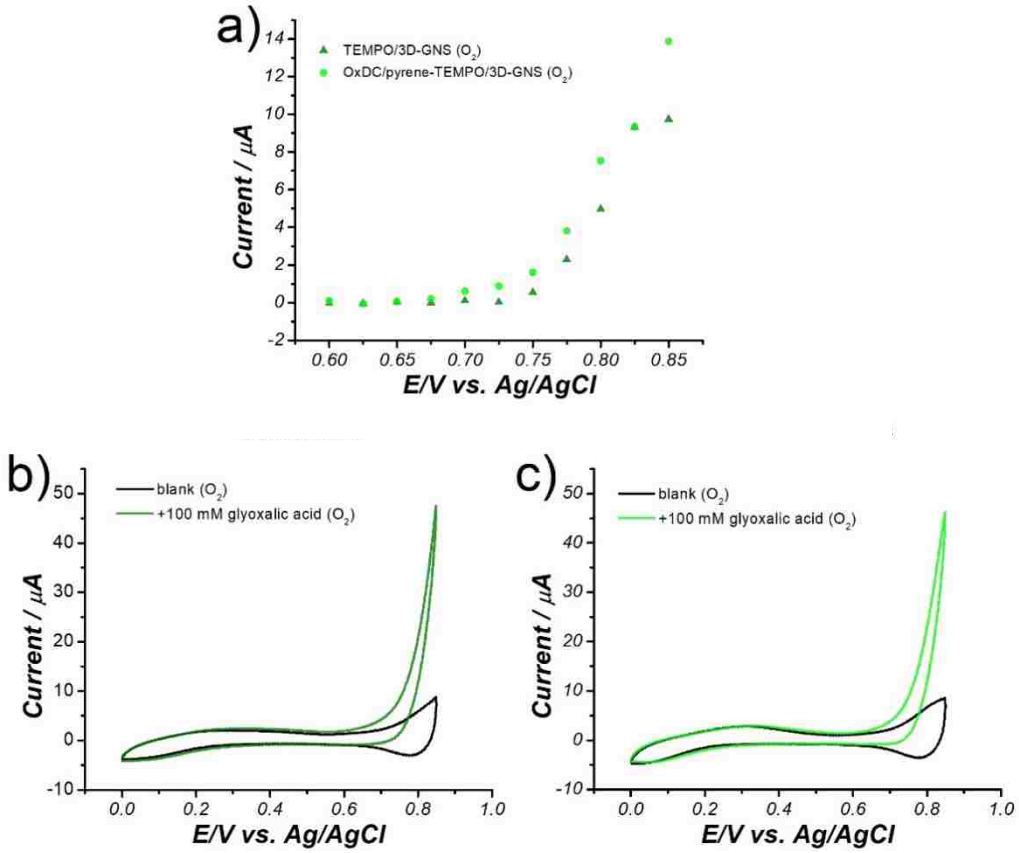

Figure 6- 9: a) activity curve in the presence of 100 mM glyoxalic acid for $OxDC_1$/pyrene-TEMPO/3D-GNS (circle) and pyrene-TEMPO/3D-GNS (triangle). CVs for b) pyrene-TEMPO/3D-GNS and c) $OxDC_1$/pyrene-TEMPO/3D-GNS in 100 mM glyoxalic acid (blue) buffered with 0.1 M CPB pH=6.2 in O_2.

Finally, the components of the hybrid catalyst are all immobilized or supported on 3D-GNS. In the presence of glyoxalic acid, the hybrid catalyst with Au (Figure 6-10b) was better than the catalyst with Pd (Figure 6-10c). There was an observable increase in the peak current when gold was substituted into the system.

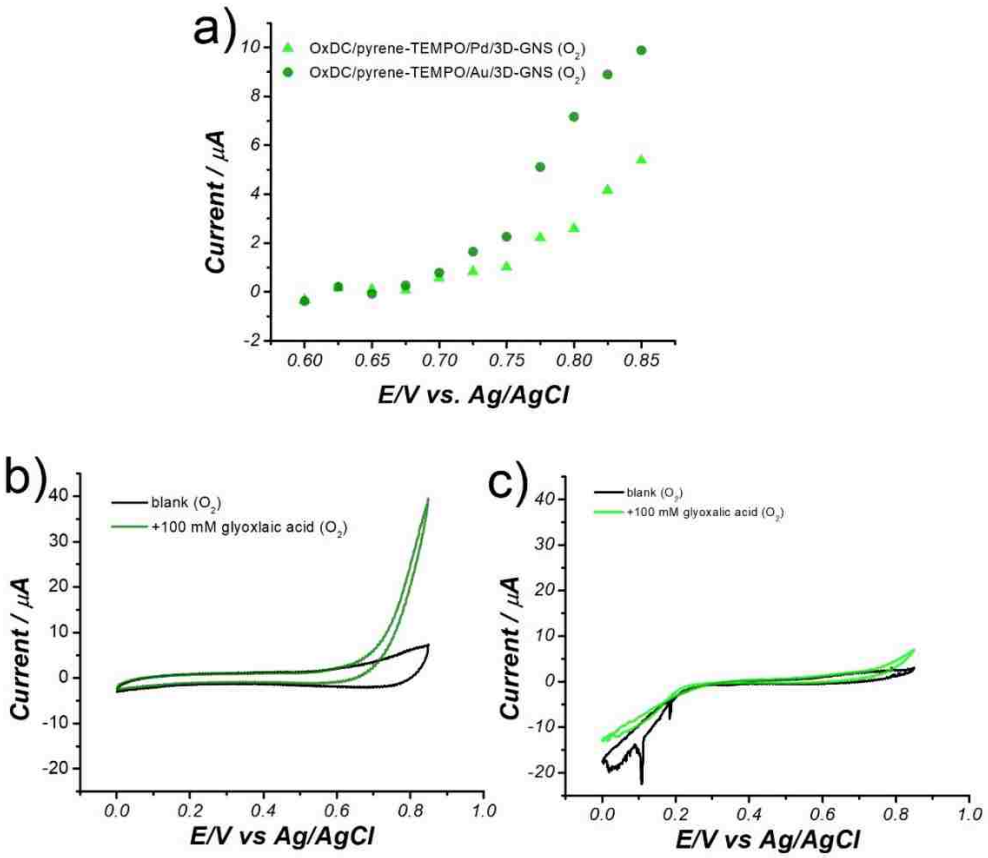

Figure 6- 10: a) activity curve of hybrid catalyst in the presence of 100 mM glyoxalic acid for $OxDC_1$/pyrene-TEMPO/Au/3D-GNS (circle) and $OxDC_1$/pyrene-TEMPO/Pd/3D-GNS (triangle). CVs for b) $OxDC_1$/pyrene-TEMPO/Au/3D-GNS and c) $OxDC_1$/pyrene-TEMPO/Pd/3D-GNS in 100 mM oxalic acid (green) buffered with 0.1 M CPB pH=6.2 in O_2.

However, CV curves are limited in the information that can be derived from them. It can be argued that it was unclear whether or not this hybrid catalyst was in fact catalyzing a multi-step cascade reaction. The next chapter describes a way to determine how OxDC/pyrene-TEMPo/Au/3D-GNS hybrid catalyst converts the substrates in the multi-step reaction.

Further work will include looking into different metallic catalysts and their incorporation in the multi-step cascade with molecular and enzymatic catalysts. In this work, gold

nanoparticles have been shown to be more selective towards the oxidation of formic acid than Pd [43] with suppressed activity towards glyoxalic acid. Furthermore, Au can oxidize formic acid at lower potentials than oxalic acid, which opens a possibility of using cell potential to ensure selectivity in the cascade. In this chapter we explored designing and engineering a synthetic multi-step cascade reaction system. The system consisting of a molecular, enzymatic, and metallic catalyst was successfully carried out on a small scale, at room temperature, in liquid phase, using glyoxalic acid as a fuel. This is the fundamental work in creating smaller multi-step reaction cascades, but it opens novel pathways for the use of multi-modal catalytic systems in different energy conversion technologies that rely on the catalysis of complex multi-step cascade reactions in designing microchemical reactors.

Chapter 7

Development of A Microchemical Reactor

Microfluid devices allow for the control of precursors to products. They are modular, take place in a liquid medium, and at room temperature. Surface Enhance Raman Spectroscopy (SERS) was used to determine the spectra of the effluent stream of the microchemical reactor by using SERS substrate. This demonstrates the integration of an electrochemical cell working on a smaller scale, in liquid phase, and at room temperature using an alternative fuel. It has been previously successfully eployed, in two instances, where the understandings of the flow and the kinetics of the catalyst have been determined by using molecular dynamics, kinetic Monte Carlo, and electrochemical paper-based analytical devices [44,45]. Having a paper-based analytical device provides a means of detecting products almost immediately after they are formed. Another advantage is extreme sensitivity of the SERS which allows for a more promising method for detecting analytes [46].

Microfluidic Reactor

The microfluidic platform was designed and engineering at the University of New Mexico by the Atanassov group [44]. Its main components comprise of the platform, made of Whatman paper, SERS detection zones, and stencil printed electrode, which mimicked a three-electrode electrochemical cell (Figure 7-1). The electrochemical experiment on the

platform were performed by holding potential at 0.8 V vs. Ag/AgCl in 0.1 M glyoxalic acid (pH=6.2) at 25°C.

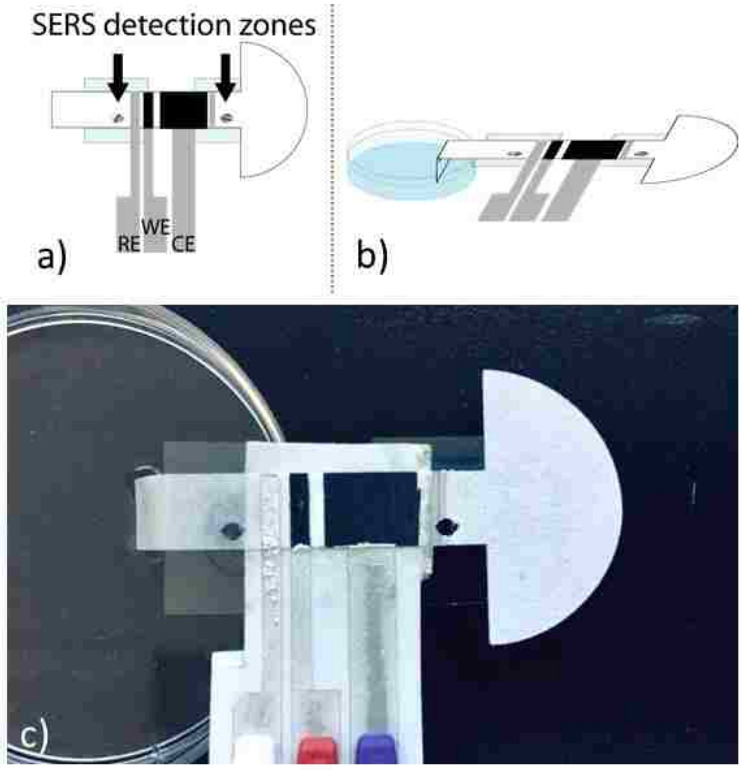

Figure 7- 1: Schematic of the microchemical reactor a) aerial view, b) oblique view, and c) photograph of an electrochemical platform

Surface-Enhanced Raman Spectroscopy (SERS)

The SERS detections zones were designed and fabricated at the University of New Mexico[44]. Stock solutions were made first. A 50 mM silver nitrate solution was made and used as the silver source. The reducing agent consisted of two solutions: one solution of 50 mM sodium borohydride and 50 mM sodium hydroxide solution. A capping agent solution consisted of 0.1% poly(vinyl alcohol)and was obtained by dissolving the PVA granules in DI water. The PVA solution was heated to 75°C for 40 minutes to promote dissolution.

The silver nanoparticles were made by adding 100 µL of the silver nitrate solution to 9.37 mL of DI water and shaken briefly to mix. To this, 30 µL of PVA solution was added. The reducing solution ($NaBH_4$ and NaOH mixture, 200 µL) was added, which was covered and shaken vigorously for 30 seconds to release H_2 gas and promote the formation of nanoparticles. This solution was pipetted onto glass coverslips in 10 µL aliquots and placed in an oven at 75°C for 20 minutes to make the SERS substrates.

Spectral Results for Hybrid Catalyst Conversion

To first determine the spectra of the products produced from the microchemical reactor, the spectrum from the reference solutions were first analyzed using the reactants. This consisted of three references, 100 mM glyoxalic acid (GA), 100 mM oxalic acid (OA) and 100 mM formic acid (FA) (Figure 7-2). The windows for the SERS detection zones allowed for analysis of the reactant and products. Each substrate has a unique spectrum and they are different from one another however, they share some similarities are similar due to their similarities in their chemical structure. The peaks were characteristic of the formation of dimers from carboxylic acid groups, monomers of carboxylic acid, alcohols, aldehydes, ketones, and formates. The substrates are 0.1 M and buffered with CPB to pH 6.2 which may cause steric hindrance and results in shifting of the peaks. For glyoxalic acid (green), the peaks unique to this substrate are at 837 cm^{-1}, 1038 cm^{-1}, 1421 cm^{-1}. For oxalic acid (blue), the first peak was bimodal where the peaks arise at 837 cm^{-1}, 904 cm^{-1}. It also has a second and third peak at 1038 cm^{-1}, and 1421 cm^{-1}, respectively. The peak in oxalic acid at 1421 cm^{-1} was noticeably higher than in glyoxalic acid. Between the two substrates, the

peak present in oxalic acid but not glyoxalic acid was at 904 cm^{-1}. Formic acid (red) has one characteristic peak at 837 cm^{-1}.

Next, the analyte mixture spectrum was determined for GA/OA, GA/FA, OA/FA, and a combination of the three, GA/OA/FA. The spectrum for GA/OA has a combination of GA and OA spectrum but the two individual spectrums do not necessarily overlap nor are they superimposable. The GA/OA spectrum has a similar low peak at 1421 cm^{-1} and another peak at 2930 cm^{-1} that was similar to the peak found in GA. Similar peaks that resembles the OA spectrum was the bimodal peak at 837 cm^{-1}, 904 cm^{-1}. The GA/FA spectrum was a combination of the two individual spectra. It still has a characteristic peak at 837 cm^{-1}, the same as GA and FA spectrum. It also has another small peak at 1421 cm^{-1}, which was visible in the GA spectra but not in the FA spectra. The OA/FA spectrum was much different than the original spectrum. There was no longer a bimodal peak at 837 cm^{-1}, 904 cm^{-1} but instead one large peak at 837 cm^{-1} which is characteristic of the FA spectra. There was also another noticeable peak at 1547 cm^{-1} and two intense peaks at 2861 cm^{-1} and 2930 cm^{-1}. These two peaks are not observable in any of the previous spectrum, which means they are unique to the OA/FA spectra. The last mixture spectrum examined was for the GA/OA/FA combination. The same peak that was prominent throughout all the spectrum was at 837 cm^{-1} however, its intensity is decreased. The same peak that appears in OA/FA appears at 1547 cm^{-1} as well as the last two peaks at 2861 cm^{-1} and 2930 cm^{-1}.

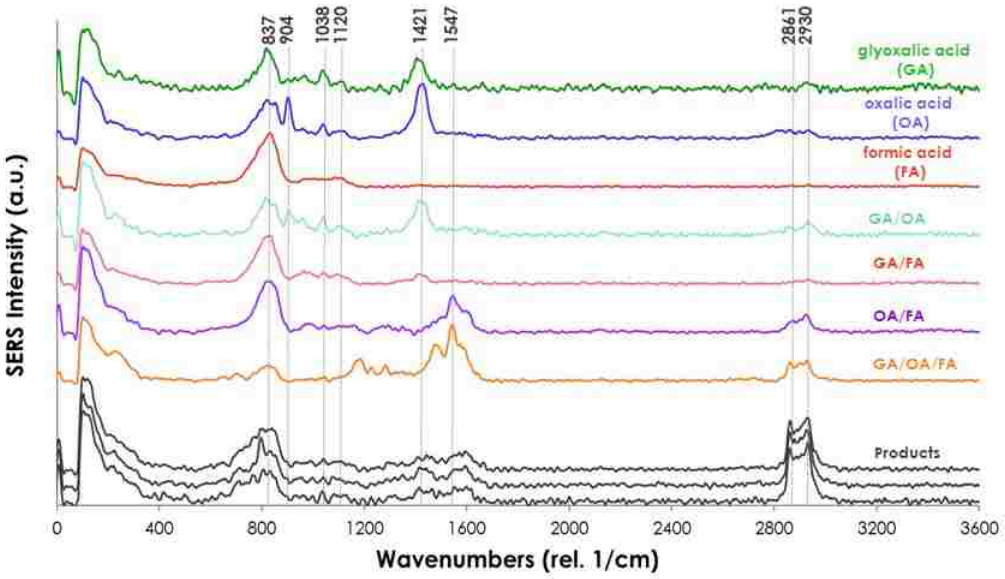

Figure 7- 2: SERS spectrum of cascade analytes and product stream (0.1 M citric phosphate buffer pH = 6.2).

The products spectra are unlike the reference spectrum. The peak at 1421 cm^{-1} was noticeable in mixtures containing glyoxalic acid, but it was suppressed in the product spectra which indicate low levels of glyoxalic acid present. The two peaks 2861 and 2931 cm^{-1} at were more pronounced which was similar to the GA/OA/FA spectrum. This was indicative of the product stream being a mixture of GA, OA, and FA, which suggests that hybrid catalyst successfully oxidized glyoxalic acid, which was then converted to oxalic acid, which was then oxidized to formic acid.

This technique not only incorporated three catalysts on a small scale, but it was also a method used to test the hybrid catalyst's ability to catalyze a multi-step cascade reaction by the means of electrochemical techniques. This was then further verified by the microchemical reactor by analyzing the spectrum of the products by using SERS with a

Raman microscope. It was confirmed that the hybrid catalyst was able to oxidize glyoxalic acid to formic acid via a three-step cascade reaction.

Chapter 8

Conclusions and Future Direction

The presented researched explored the incorporation of the three catalysts with three different modalities, molecular, enzymatic, and metallic catalyst on the same support. This allows for novel pathways to be further explored and expanded towards the catalysis of multi-step reactions by interchanging any of the three catalytic components. An immobilization technique based on the tethering of the large multimeric enzyme on the carbon-based supports was further developed. The efficiency of the immobilized procedure was tested using a UV-visible based FDH assay. The developed immobilized approach can be translated to other enzymes, whether they are large (hexameric) or smaller. Successful immobilization was accomplished on both a simple carbonaceous support, MWNT, as well as on a complex carbonaceous support, 3D-GNS. The approach can therefore be used not only for different enzymes but also for different carbon-based supports. The molecular catalyst was successfully immobilized on 3D-GNS by modifying it with a pyrene moiety. This procedure enables immobilization of the molecular catalysts close to other catalysts in the cascade. In addition, a hybrid enzymatic-molecular catalyst was designed, using the same immobilization technique, and was used to catalyze a two-step reaction. Enzymatic systems convert oxalic acid to formic acid, and the molecular system further oxidizes formic acid to CO2, which was confirmed using electrochemical methods. This allowed for the integration of a third catalysts of a different modality from the first two catalysts. The design of the hybrid molecular-enzymatic-metallic catalyst allows for further exploration of interchanging the catalysts. For example, interchanging palladium for gold,

which allowed for a higher selectivity of the metallic catalyst in the cascade. However, the exploration of optimal the metallic catalyst can be further tested. Finally, a technique was used to confirm the conversion of the reactants to products in the hybrid cascade by using a spectro-electrochemical platform.

This proposal explores the fundamental science behind developing hybrid catalysts of three different modalities and their use in multi-step catalytic reaction on s small scale in liquid media. This work also provides basis for further improvements in the synthetic catalytic cascades, which would lead to the increase in their efficiency and allow more control over the catalytic process. One of the options is the exploration of surface-bound diffusion as a way to create more effective transport of intermediates in the cascade. This can be done by modifying the carbonaceous support by doping the support with nitrogen or boron. The change in the surface charge of the support has the potential to keep intermediates close to the surface and within the vicinity of the next catalyst allowing for more efficient transport and conversion by the next catalyst downstream in the synthetic cascade. Molecular dynamics simulations can also be used to explore the positioning of the enzyme when it is immobilized to the support. This will help further optimize the tether and enzyme concentration to avoid enzyme emulsification. Furthermore, characterization of the created molecular-enzymatic-metallic system by fluorescence microscopy techniques would help us understand how the enzymatic catalyst is distributed on the support and enable us to start understanding the structure to function properties of these complex systems. This research also opens pathways to develop and engineer more complex synthetic hybrid catalysts for larger multi-step cascade reactions as well as the development of more

sophisticated microchemical reactors, which include using different catalyst and different alternative fuels.

Appendix

A1 CV of Pd/3D-GNS in 0.1 M citric phosphate buffer pH = 6.2 (black) and 100 mM a) oxalic acid, b) glyoxalic acid and c) formic acid purged in N_2.

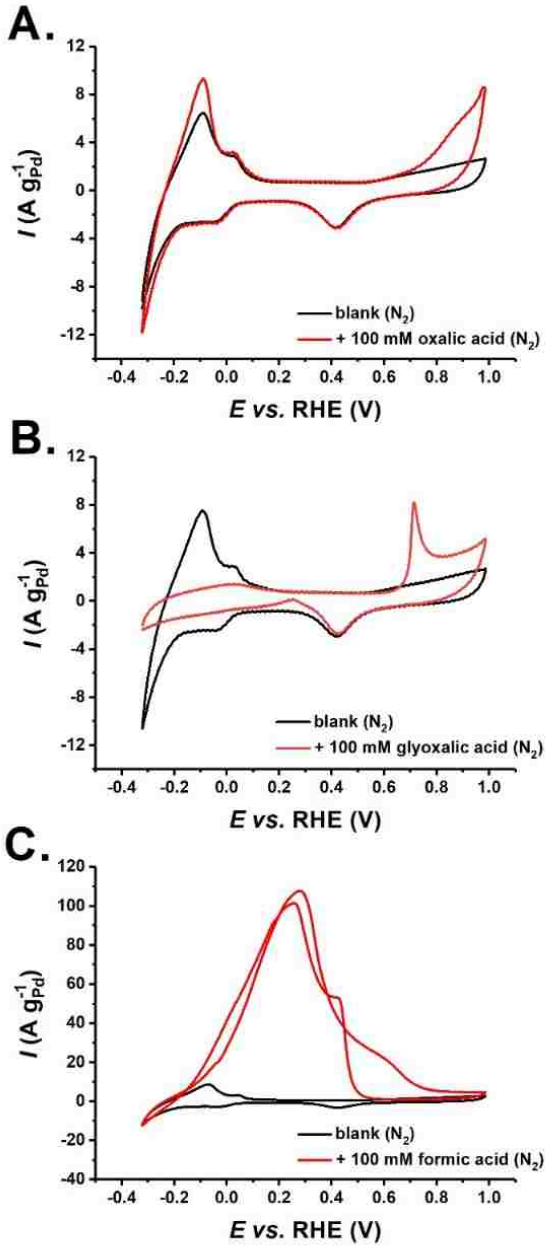

A2 Electrocatalytical activity summary of Pd/3D-GNS towards formic acid

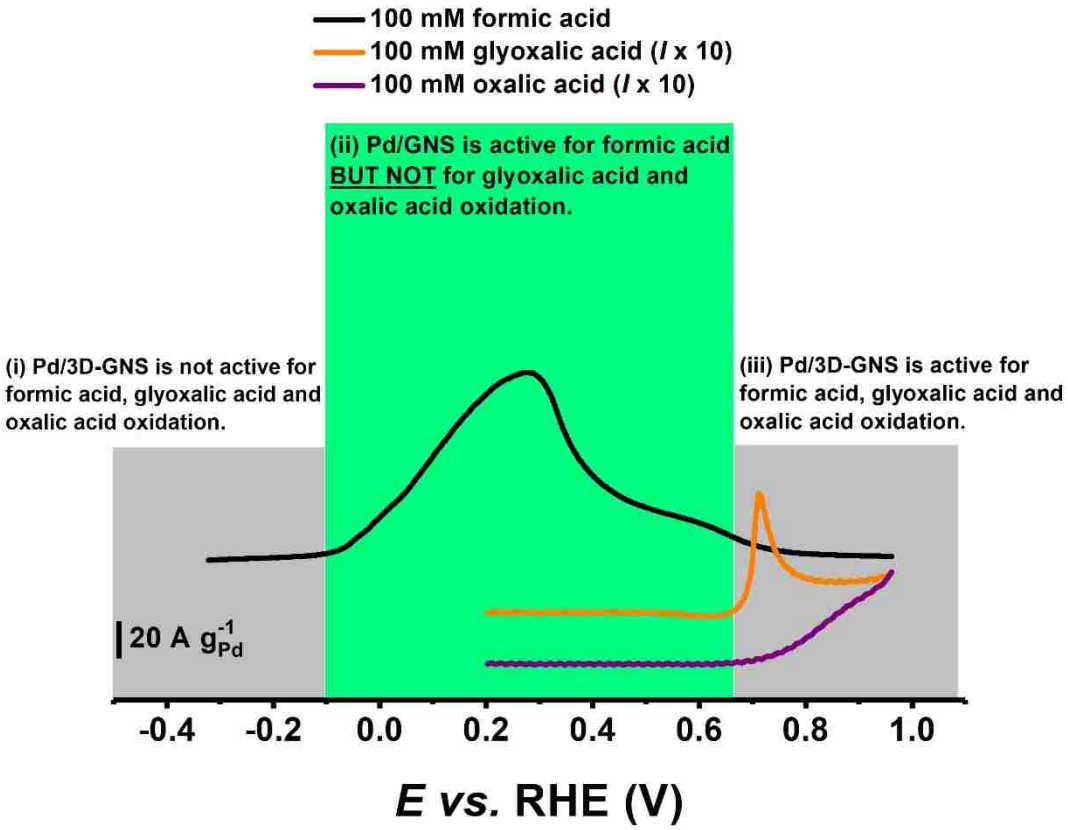

A3 CV curves of FXC-400 in GA, OA, and FA

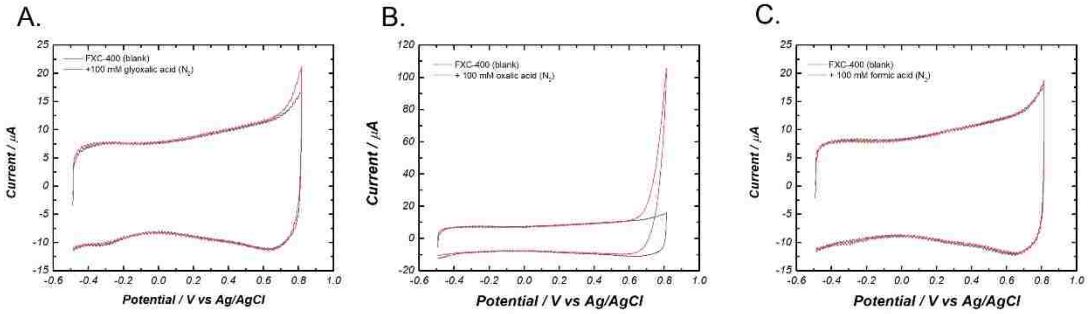

References

1. Rustagi N, Satyapal S. by Bryan Pivovar, Neha Rustagi, and Sunita Satyapal. 2019.

2. Wheeldon I, Minteer SD, Banta S, Barton SC, Atanassov P, Sigman M. Substrate channelling as an approach to cascade reactions. *Nat Chem*. 2016;8(4):299-309. doi:10.1038/nchem.2459.

3. Zhang YP. Substrate channeling and enzyme complexes for biotechnological applications. *Biotechnol Adv*. 2011;29(6):715-725. doi:10.1016/j.biotechadv.2011.05.020.

4. Qi J, Xin L, Chadderdon DJ, et al. Electrocatalytic selective oxidation of glycerol to tartronate on Au/C anode catalysts in anion exchange membrane fuel cells with electricity cogeneration. *Appl Catal B Environ*. 2014;154-155:360-368. doi:10.1016/j.apcatb.2014.02.040.

5. Simões M, Baranton S, Coutanceau C. Electro-oxidation of glycerol at Pd based nano-catalysts for an application in alkaline fuel cells for chemicals and energy cogeneration. *Appl Catal B Environ*. 2010;93(3-4):354-362. doi:10.1016/j.apcatb.2009.10.008.

6. Arechederra RL, Minteer SD. Complete Oxidation of Glycerol in an Enzymatic Biofuel Cell. *Fuel Cells*. 2009;9(1):63-69. doi:10.1002/fuce.200800029.

7. Arechederra RL, Minteer SD. Kinetic and transport analysis of immobilized oxidoreductases that oxidize glycerol and its oxidation products. *Electrochim Acta*. 2010;55(26):7679-7682. doi:10.1016/j.electacta.2009.09.083.

8. Sokic-Lazic D, Arechederra RL, Treu BL, Minteer SD. Oxidation of biofuels: Fuel diversity and effectiveness of fuel oxidation through multiple enzyme cascades. *Electroanalysis*. 2010;22(7-8):757-764. doi:10.1002/elan.200980010.

9. Srere P. Complexes Of Sequential Metabolic Enzymes. *Annu Rev Biochem*. 1987;56(1):89-124. doi:10.1146/annurev.biochem.56.1.89.

10. Pröschel M, Detsch R, Boccaccini AR, Sonnewald U. Engineering of Metabolic Pathways by Artificial Enzyme Channels. *Front Bioeng Biotechnol*. 2015;3(October):1-13. doi:10.3389/fbioe.2015.00168.

11. Moehlenbrock MJ, Toby TK, Waheed A, Minteer SD. Metabolon Catalyzed Pyruvate / Air Biofuel Cell. *J Am Chem Soc*. 2010;132:6288-6289. doi:Doi 10.1021/Ja101326b.

12. Salavagione HJ, Garc P, Morall E, Barbero C. Spectroelectrochemical study of the oxidation of aminophenols on platinum electrode in acid medium n. 2004;565:375-

383. doi:10.1016/j.jelechem.2003.11.005.

13. Lović JD, Tripković A V., Gojković SL, et al. Kinetic study of formic acid oxidation on carbon-supported platinum electrocatalyst. *J Electroanal Chem*. 2005;581(2):294-302. doi:10.1016/j.jelechem.2005.05.002.

14. Serov A, Asset T, Padilla M, et al. Highly-active Pd-Cu electrocatalysts for oxidation of ubiquitous oxygenated fuels. *Appl Catal B Environ*. 2016;191:76-85. doi:10.1016/j.apcatb.2016.03.016.

15. Bianchini C. Palladium-Based Electrocatalysts for Alcohol Oxidation in Direct Alcohol Fuel Cells. *Interfacial Phenom Electrocatal*. 2011;51:203-253. doi:10.1007/978-1-4419-5580-7_4.

16. Antolini E. Palladium in fuel cell catalysis. *Energy Environ Sci*. 2009;2(9):915. doi:10.1039/b820837a.

17. Perry A, Kabir S, Matanovic I, et al. Novel Hybrid Catalyst for the Oxidation of Organic Acids: Pd Nanoparticles Supported on Mn-N-3D-Graphene Nanosheets. *ChemElectroChem*. 2017:1-10. doi:10.1002/celc.201700285.

18. Abdellaoui S, Seow Chavez M, Matanovic I, et al. Hybrid molecular/enzymatic catalytic cascade for complete electro-oxidation of glycerol using a promiscuous NAD-dependent formate dehydrogenase from Candida boidinii. *Chem Commun*. 2017;54:978-979. doi:10.1039/C7CC01027C.

19. Hickey DP, McCammant MS, Giroud F, Sigman MS, Minteer SD. Hybrid enzymatic and organic electrocatalytic cascade for the complete oxidation of glycerol. *J Am Chem Soc*. 2014;136(45):15917-15920. doi:10.1021/ja5098379.

20. Abdellaoui S, Hickey DP, Stephens AR, Minteer SD. SI: Recombinant oxalate decarboxylase: enhancement of a hybrid catalytic cascade for the complete electro-oxidation of glycerol. *Chem Commun*. 2015;51(76):14330-14333. doi:10.1039/C5CC06131H.

21. Chen J, Yao B, Li C, Shi G. An improved Hummers method for eco-friendly synthesis of graphene oxide. *Carbon N Y*. 2013;64(1):225-229. doi:10.1016/j.carbon.2013.07.055.

22. Serov A, Martinez U, Atanassov P. Electrochemistry Communications Novel Pd – In catalysts for alcohols electrooxidation in alkaline media. *Electrochem commun*. 2013;34:185-188. doi:10.1016/j.elecom.2013.06.003.

23. Reinhardt L, Svedruzic D, Chang C, Cleland W, Richards N. Heavy atom isotope effects on the reaction catalyzed by the oxalate decarboxylase from *Bacillus subtilis*. *J Am Chem Soc*. 2003;125(5):1244-1252. doi:10.1021/ja0286977.

24. Svedružić D, Jónsson S, Toyota CG, et al. The enzymes of oxalate metabolism:

Unexpected structures and mechanisms. *Arch Biochem Biophys*. 2005;433(1):176-192. doi:10.1016/j.abb.2004.08.032.

25. Lin R, Wu R, Huang X, Xie T. Immobilization of Oxalate Decarboxylase To Eupergit and Properties of the Immobilized Enzyme. *Prep Biochem Biotechnol*. 2011;41(2):154-165. doi:10.1080/10826068.2011.547350.

26. Twahir U, Molina L, Ozarowski A, Angerhofer A. Immobilization of Bacillus subtilis oxalate decarboxylase on a Zn-IMAC resin. *Biochem Biophys Reports*. 2015;4:98-103. doi:10.1016/j.bbrep.2015.08.017.

27. Kobos RK, Ramsey TA. Enzyme electrode system for oxalate determination utilizing oxalate decarboxylase immobilized on a carbon dioxide sensor. *Anal Chim Acta*. 1980;121(C):110-118. doi:10.1016/S0003-2670(01)84405-6.

28. Matanovic I, Babanova S, Chavez MS, Atanassov P. Protein-Support Interactions for Rationally Designed Bilirubin Oxidase Based Cathode: A Computational Study. *J Phys Chem B*. 2016;120(15):3634-3641. doi:10.1021/acs.jpcb.6b01616.

29. Babanova S, Matanovic I, Chavez MS, Atanassov P. Role of Quinones in Electron Transfer of PQQ-Glucose Dehydrogenase Anodes - Mediation or Orientation Effect. *J Am Chem Soc*. 2015;137(24):7754-7762. doi:10.1021/jacs.5b03053.

30. Lopez RJ, Babanova S, Artyushkova K, Atanassov P. Surface modifications for enhanced enzyme immobilization and improved electron transfer of PQQ-dependent glucose dehydrogenase anodes. *Bioelectrochemistry*. 2015;105:78-87. doi:10.1016/j.bioelechem.2015.05.010.

31. Fernandez-Lafuente R. Stabilization of multimeric enzymes: Strategies to prevent subunit dissociation. *Enzyme Microb Technol*. 2009;45(6-7):405-418. doi:10.1016/j.enzmictec.2009.08.009.

32. Kabir S, Serov A, Artyushkova K, Atanassov P. Design of Novel Graphene Materials as a Support for Palladium Nanoparticles: Highly Active Catalysts towards Ethanol Electrooxidation. *Electrochim Acta*. 2016;203:144-153. doi:10.1016/j.electacta.2016.04.026.

33. Serov A, Andersen NI, Kabir SA, et al. Palladium Supported on 3D Graphene as an Active Catalyst for Alcohols Electrooxidation. *J Electrochem Soc*. 2015;162(12):F1305-F1309. doi:10.1149/2.0301512jes.

34. Kabir S, Artyushkova K, Serov A, Kiefer B, Atanassov P. Binding energy shifts for nitrogen-containing graphene-based electrocatalysts - Experiments and DFT calculations. *Surf Interface Anal*. 2016;48(5):293-300. doi:10.1002/sia.5935.

35. Hickey DP, Schiedler DA, Matanovic I, et al. Predicting Electrocatalytic Properties: Modeling Structure-Activity Relationships of Nitroxyl Radicals. *J Am Chem Soc*. 2015;137(51):16179-16186. doi:10.1021/jacs.5b11252.

36. Bonet F, Delmas V, Grugeon S, Urbina RH, Silvert P. SYNTHESIS OF MONODISPERSE Au , Pt , Pd , Ru AND Ir NANOPARTICLES IN ETHYLENE GLYCOL. 2000;11(8):1277-1284.

37. Synthesis of monodisperse submicronic gold particles by the polyol process. 1995;2738(95).

38. Kabir S, Serov A, Zadick A, Artyushkova K, Atanassov P. Palladium Nanoparticles Supported on Three-Dimensional Graphene Nanosheets: Superior Cathode Electrocatalysts. *ChemElectroChem*. 2016;3(10):1655-1666. doi:10.1002/celc.201600245.

39. Tremiliosi-filho G, Gonzalez ER, Motheo AJ, Belgsir EM, Le J. Electro-oxidation of ethanol on gold : analysis of the reaction products and mechanism. 1998;444:31-39.

40. Poitiers U De. OXIDATION OF ORGANIC COMPOUNDS ON NOBLE METALS IN AQUEOUS. 1984:1581-1588.

41. Beden B, Cetin I. Electrocatalytic Oxidation of Saturated Oxygenated on Gold Electrodes ’. 1987;46:37-46.

42. Nørskov JK, Rossmeisl J, Logadottir A, Lindqvist L, Lyngby D-, Jo H. Origin of the Overpotential for Oxygen Reduction at a Fuel-Cell Cathode. 2004:17886-17892. doi:10.1021/jp047349j.

43. Rodrigues EG, Carabineiro SAC, Delgado JJ, Chen X, Pereira MFR, Órfão JJM. Erratum: Gold supported on carbon nanotubes for the selective oxidation of glycerol (Journal of Catalysis 285 (2012) (83-91)). *J Catal*. 2012;292:246-247. doi:10.1016/j.jcat.2012.05.016.

44. Hickey DP. Spectro-Electrochemical Microfluidic Platform for Monitoring Multi-Step Cascade Reactions. 2019:246-251. doi:10.1002/celc.201800578.

45. Liu Y, Matanovic I, Hickey DP, Minteer SD, Atanassov P, Barton SC. Cascade Kinetics of an Artificial Metabolon by Molecular Dynamics and Kinetic Monte Carlo. *ACS Catal*. 2018;8:7719-7726. doi:10.1021/acscatal.8b01041.

46. Schlücker S. Surface-Enhanced Raman Spectroscopy : Concepts and Chemical Applications Angewandte. 2014:4756-4795. doi:10.1002/anie.201205748.